

Solution for volume reflection of ultra-relativistic particles in a bent crystal

M.V. Bondarenco*

Kharkov Institute of Physics and Technology, 1 Academic St., 61108 Kharkov, Ukraine

(Dated: April 23, 2019)

For trajectory of a positively or a negatively charged particle undergoing volume reflection in a bent crystal an exact analytic expression is derived, within a model of parabolic continuous potential in each inter-planar interval, and with the neglect of multiple scattering. In the limit of bending radius greatly exceeding the critical value, formulas are obtained for the particle mean deflection angle in units of Lindhard's critical angle, and for the scattered beam profile. Volume reflection of negatively charged particles is shown to contain effects of rainbow scattering and orbiting, whereas with positively charged particles none of such effects arise within the given model.

PACS numbers: 61.85.+p, 29.27.-a, 45.10.-b

Keywords: volume reflection; harmonic potential; rainbow scattering; orbiting

I. INTRODUCTION

Volume reflection effect is the deflection of a beam of high-energy charged particles upon their *over-barrier* (non-channeled) passage through a planarly oriented bent crystal. The effect becomes manifest at crystal bending radius R large compared with the critical value R_c . This is the same condition as for feasibility of channeling in the bent crystal [1], but the regime of particle motion in the crystal yet depends on the angle of entry relative to active atomic planes, i. e. on the particle "transverse energy". When the beam entry angle by far exceeds the critical value θ_c , then, moving in the continuous potential of bent planes, conserving the particle full transverse (radial) energy, the particles get captured into channels rarely (through incoherent scattering on atomic electrons and nuclei), and mostly get reflected through the volume reflection mechanism. Curiously, in the latter case deflection proceeds to the side *opposite* to that of the crystal bending; the value of the deflection angle is of the order of critical angle θ_c . That phenomenon was discovered in numerical simulations 2 decades ago [2] and recently verified experimentally [3]. Yet, after the deflection the beam remains fairly well collimated, i. e. the angular dispersion is indeed much smaller than the mean deflection, which inspired propositions to utilize it for beam collimation and partial extraction at ultra-relativistic charged particle accelerators [4].

The classical [14] dynamics to deal with in the problem of volume reflection basically reduces to particle motion in a cylindrically-symmetrical continuous potential of bent atomic planes. Therewith, granted the angular momentum conservation, the final deflection angle expresses standardly as an integral over the radial coordinate from an inverse square root function involving the potential (see Eq. (55b) below). But as the integration extends over many inter-planar intervals, the common practice so far was to evaluate it only numerically [5].

Unfortunately, the purely numerical, computer approach, although indispensable at simulation of specific experiments, is inferior in transparency to analytical methods, especially in what concerns description of multi-parameter dependencies (specifically, on the particle energy and impact parameter), and singularity features. Furthermore, an analytic expression for the entire trajectory would be helpful if one aims to calculate the accompanying processes, such as electromagnetic radiation [6]. In this regard, it seems worth providing ourselves with some simply calculable model of particle motion in the potential field of bent atomic planes. Particularly, one may take the opportunity that the inter-planar potential in a silicon crystal, at least in the orientation (110), is fairly close to parabolic shape (see, e. g., Ref. 2 of [2]). A parabolic (harmonic) potential represents a linear oscillator and admits a simple solution for the particle trajectory within a single inter-planar interval. The non-trivial part of the problem is then to connect solutions on the boundaries of the adjacent intervals, and furthermore, manage doing that transitively, i. e. simultaneously for an arbitrary number of the adjacent intervals.

In the present work, we will deliver a solution for the posed model problem, expressing the particle trajectory upon its passage through an arbitrary number of inter-planar intervals. From this solution, the particle final deflection angle derives in terms of a sum of inverse trigonometric (for positively charged particles) or hyperbolic (for negatively charged particles) functions. Those representations are exact for any ratio R/R_c . In the case $R \gg R_c$, most interesting in relation to volume reflection and practical applications, the sums involved may be replaced by integrals via the Euler-Maclaurin formula, and the integrals be done in a closed form. As a result, one arrives at fairly simple formulas for the deflection angle dependence on the critical angle, on the ratio R/R_c , and on the impact parameter. The analytic approach also automatically produces correct singularity features of the differential cross-section, such as rainbow scattering and orbiting, in the case of volume reflection of negative particles, whence for positively charged particles such singularities do not develop within our model.

*Electronic address: bon@kipt.kharkov.ua

The outline of the paper is as follows. In Sec. II we implement the procedure of solution connection between adjacent inter-planar intervals, and express the particle trajectory as function of the interval order number. In Sec. III we determine the reflection point location and evaluate the particle reflection angle for an arbitrary ratio R/R_c . In Sec. IV we scrutinize the limit $R \gg R_c$ of our primary interest, first for positively, then for negatively charged particles. From the found indicatrix function, we evaluate the scattering differential cross-section as a function of the reflection angle variation relative to the mean value. Secs. III and IV appear to be technical, but the calculations are elementary. In Sec. V we comment on the opposite limit $R \ll R_c$. In Sec. VI we analyze experimental implications of the given theory. A summary is given in Sec. VII.

II. PARTICLE TRAJECTORY IN A BENT CRYSTAL

A. Initial conditions

The usual geometry of experiments on volume reflection is an impact of a charged particle beam normally to a thin [15], weakly bent crystal plate. The practically unavoidable slight curvature of the crystal boundary thereat is of minor consequence, since the main contribution to the particle reflection angle comes from a vicinity of some point in the depth of the crystal. For definiteness and to establish an easy connection with the particle impact parameter in the initial (perfectly collimated [16]) beam, let us consider a particle incident along the z axis on a crystal whose front face is a *perfect plane*, located at $z = 0$. As for the crystal rear face, for our purposes in this paper we can leave it unspecified at all, as if the crystal was infinitely thick. Then, let $\theta_0 > 0$ be the (small) angle of inclination of crystalline planes to the z -axis at the crystal front face (see Fig. 1), and let x -axis, perpendicular to Oz , point in the direction of the crystal bend. Moving at small angles to the crystal planes, the particle interacts most strongly (coherently) with the averaged, so-called continuous inter-planar potential [7], which induces a force with dominant x -component (yet slowly dependent on z) [17]. Along the y coordinate there is a translational invariance, ensuring conservation of y -component of the particle momentum.

In monocrystals of not too heavy chemical elements, in particular for silicon (having a diamond-type lattice), in planar orientation (110) the continuous potential in each inter-planar interval may closely be approximated by a quadratic function, as we had mentioned in the Introduction [18]. That entails a linear equation of motion for the classical [14] ultra-relativistic [19] particle:

$$\ddot{x} = \frac{2F_{\max}}{Ed} (-x + x_0), \quad (1)$$

$$t \approx z, \quad (c = 1, \text{ small angle motion}) \quad (2)$$

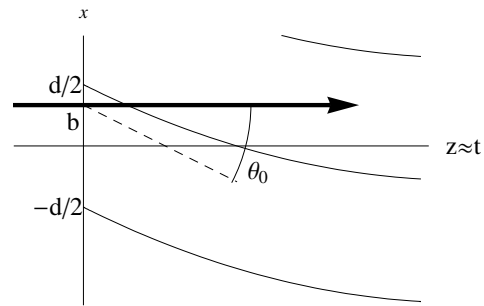


FIG. 1: Variables describing the particle parameters at the entrance to the bent crystal.

where x_0 is the midpoint of the inter-planar interval, d the inter-planar distance, E the particle energy, and F_{\max} the force acting on the particle at the edge of the inter-planar interval $x - x_0 = -\frac{d}{2}$. For positively charged particles F_{\max} is positive, whereas for negatively charged particles it is negative. Note that the force and the particle energy enter equation (1) only through the ratio

$$\frac{E}{|F_{\max}|} = R_c, \quad (3)$$

known as the Tsyganov critical radius [1]. It is also appropriate to introduce a time unit

$$\tau = \sqrt{\frac{Ed}{2|F_{\max}|}} \equiv \sqrt{\frac{R_c d}{2}} \quad (4)$$

($2\pi\tau$ has the meaning of the period of positive charged particle channeling, although herein we deal not with channeling but with an over-barrier motion).

The only consequence of the crystal bending is that x_0 in Eq. (1) acquires dependence on the longitudinal coordinate z , which for ultra-relativistic motion under small angles to Oz may be equated to the current time t :

$$x_0 = x_0(z \approx t). \quad (\text{the crystal bend function}) \quad (5)$$

In application to volume reflection, we are interested in the uniform bending of the crystal, at which $x_0(t)$ describes a circular arc of a small opening angle. That small arc may equally well be approximated by a parabola, and hence $x_0(t)$ is determined by the equation

$$x_0(t) = -\theta_0 t + \frac{t^2}{2R}, \quad (\text{uniformly bent crystal}) \quad (6)$$

where R is the atomic plane bending radius (without the loss of generality one may let $x_0(0) = 0$ – see Fig. 1). Inserting (6 to (1)), and implementing (4), we get the particle equation of motion in the first inter-planar interval:

$$\ddot{x} = \pm \frac{1}{\tau^2} \left(-x - \theta_0 t + \frac{t^2}{2R} \right). \quad \left\{ \begin{array}{l} \text{pos. charged particles} \\ \text{neg. charged particles} \end{array} \right\} \quad (7)$$

Initial conditions for $x(t)$ stand as

$$x(0) = b, \quad (8)$$

$$\dot{x}(0) = 0, \quad (9)$$

where b , restricted to the interval

$$-\frac{d}{2} \leq b \leq \frac{d}{2}, \quad (10)$$

is the impact parameter measured from the middle of the interval

The equations of motion further simplify in terms of the “subtracted radius” variable

$$r(t) = -x(t) - \theta_0 t + \frac{t^2}{2R}, \quad (11)$$

becoming

$$\ddot{r} = \frac{\delta \mp r}{\tau^2}, \quad \left(\text{in } -\frac{d}{2} \leq r \leq \frac{d}{2} \right) \quad (12)$$

where

$$\delta = \frac{\tau^2}{R}. \quad (13)$$

Thus, $\pm\delta$ is the spatial shift of the oscillator equilibrium position due to the crystal bend, i. e., due to the centrifugal force, which in the present small-angle approximation, presuming condition $r \ll R$ within the weakly bent crystal, is treated as virtually independent of the subtracted radius r (cf. [2]). For $r(t)$, the initial conditions (8-9) translate to

$$r(0) = -b, \quad (14)$$

$$\dot{r}(0) = -\theta_0. \quad (15)$$

Eq. (12) describes a conservative harmonic oscillator with a shifted equilibrium position, whose general solution reads:

$$r = \pm\delta - A_0 \left\{ \frac{\sin}{\sinh} \right\} \left(\frac{t}{\tau} + \varphi_0 \right). \quad (16)$$

(Here and henceforth upper signs and figures refer to positively charged particles, and lower ones – to negatively charged particles.) Matching initial conditions (14-15) allows one to determine constants A_0 and φ_0 :

$$A_0 = \sqrt{\tau^2 \theta_0^2 \pm (b \pm \delta)^2}, \quad (17)$$

$$\varphi_0 = \left\{ \frac{\arcsin}{\text{arsinh}} \right\} \frac{b \pm \delta}{A_0} \quad (18)$$

(the sign of A_0 must be chosen positive in order that $\dot{r}(0)$ at $\theta_0 > 0$, according to (15), was negative).

Further on, solution (16) is to be connected with solutions in the subsequent inter-planar intervals. Importantly, since these solutions have to be connected at a definite r , the condition of connection will not depend on the current phase of the harmonic motion, such as φ_0 in Eq. (16), as we are going to show.

B. Connection of solutions in adjacent intervals

After having entered the crystal, the particle crosses the next inter-planar interval border $r = -\frac{d}{2}$ at an instant

$$\frac{t_1}{\tau} = \left\{ \frac{\arcsin}{\text{arsinh}} \right\} \frac{\frac{d}{2} \pm \delta}{A_0} - \varphi_0 \quad (19)$$

(inferred from (16) by letting $r = -\frac{d}{2}$ and solving for t). At this instant, the equation of particle motion turns to

$$\ddot{r} = \frac{\delta \mp (d+r)}{\tau^2} \quad \left(\text{in } -\frac{3d}{2} \leq r \leq -\frac{d}{2} \right). \quad (20)$$

That is again a harmonic oscillator, merely with an altered equilibrium position, and general solution of (20) may be written as

$$r_1(t) = \pm\delta - d - A_1 \left\{ \frac{\sin}{\sinh} \right\} \left(\frac{t}{\tau} + \varphi_0 + \Delta\varphi_1 \right). \quad (21)$$

Values of new constants A_1 , $\Delta\varphi_1$ are now to be determined from the continuity of $r(t)$ and $\dot{r}(t)$ at the boundary point $r = -\frac{d}{2}$. That can be done without formally solving the system of two equations. First, compare two energy integrals of motion

$$A_1^2 = \tau^2 \dot{r}_1^2 \pm (\pm\delta - d - r_1)^2 \quad (22)$$

$$A_0^2 = \tau^2 \dot{r}^2 \pm (\pm\delta - r)^2 \quad (23)$$

in their common point, where $r = r_1 = -\frac{d}{2}$, $\dot{r} = \dot{r}_1$. Subtracting (23) from (22), one gets $A_1^2 = A_0^2 - 2\delta d$, i. e.

$$A_1 = \sqrt{A_0^2 - 2\delta d}. \quad (24)$$

Thereupon, the phase shift $\Delta\varphi_1$ is sought from a condition $r_1(t_1) = -\frac{d}{2}$. One finds:

$$\Delta\varphi_1 = - \left\{ \frac{\arcsin}{\text{arsinh}} \right\} \frac{\frac{d}{2} \pm \delta}{A_0} - \left\{ \frac{\arcsin}{\text{arsinh}} \right\} \frac{\frac{d}{2} \mp \delta}{A_1} \quad (25)$$

(for a geometric explanation of this relation for positive particles – see Fig. 2). As we had expected, neither A_1 , nor $\Delta\varphi_1$ depends on φ_0 .

At each next boundary connection of the solutions is implemented in exactly the same way. Writing in the n -th interval

$$r_n(t) = \pm\delta - nd - A_n \left\{ \frac{\sin}{\sinh} \right\} \left(\frac{t}{\tau} + \varphi_0 + \sum_{m=1}^n \Delta\varphi_m \right), \quad (26)$$

$$\left(-\frac{d}{2} - nd \leq r \leq \frac{d}{2} - nd, \quad t_n \leq t \leq t_{n+1} \right)$$

the generic amplitude is found as

$$\begin{aligned} A_n &= \sqrt{A_{n-1}^2 - 2\delta d} = \sqrt{A_0^2 - 2n\delta d} \\ &= \sqrt{\tau^2 \theta_0^2 \pm (b \pm \delta)^2 - 2n\delta d}. \end{aligned} \quad (27)$$

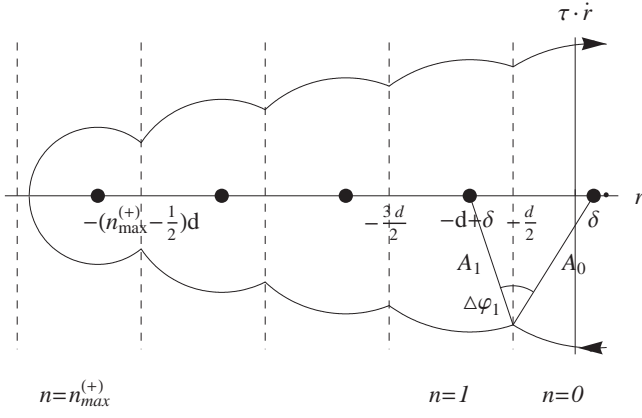


FIG. 2: Solid curve – the phase-space (the subtracted radius r vs. the radial velocity \dot{r}) trajectory for positively charged particles, under condition $\frac{d}{2} > \delta$. Dashed vertical lines signify the positions of bent atomic planes (definite r). Thick dots indicate centers of the trajectory circular segments. Vertex angle $\Delta\varphi_1$ (and similarly all other $\Delta\varphi_n$) may be interpreted as a geometric sum of vertex angles in a pair of right triangles having a common cathetus, and with the unequal catheti equal $\frac{d}{2} + \delta$, $\frac{d}{2} - \delta$, and the hypotenuses A_0 , A_1 .

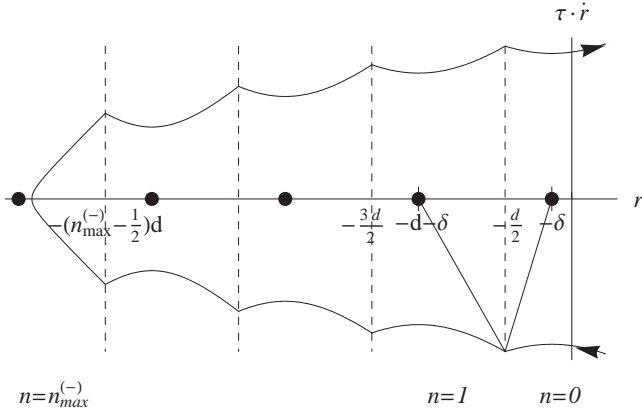


FIG. 3: The same as Fig. 2, but for negatively charged particles, assuming condition $\delta < \frac{d}{2}$ (see Sec. III B).

and the phase shift is deduced to be

$$\Delta\varphi_n = - \left\{ \begin{array}{c} \arcsin \\ \operatorname{arsinh} \end{array} \right\} \frac{\frac{d}{2} \pm \delta}{A_{n-1}} - \left\{ \begin{array}{c} \arcsin \\ \operatorname{arsinh} \end{array} \right\} \frac{\frac{d}{2} \mp \delta}{A_n}, \quad (28)$$

where the amplitudes in the denominators must be regarded as already known. The instants of border passage can also be evaluated:

$$\frac{t_n}{\tau} = \sum_{m=1}^n \left\{ \begin{array}{c} \arcsin \\ \operatorname{arsinh} \end{array} \right\} \frac{\frac{d}{2} \pm \delta}{A_{m-1}} + \sum_{m=1}^{n-1} \left\{ \begin{array}{c} \arcsin \\ \operatorname{arsinh} \end{array} \right\} \frac{\frac{d}{2} \mp \delta}{A_m} - \left\{ \begin{array}{c} \arcsin \\ \operatorname{arsinh} \end{array} \right\} \frac{b \pm \delta}{A_0}. \quad (r_{n-1} \rightarrow r_n) \quad (29)$$

A relevant warning is that amplitudes A_n should not be regarded as a measure of the particle spatial wiggling

in each interval. As Figs. 2, 3 indicate, the trajectory swinging *enhances* as the particle penetrates deeper into the crystal, whereas amplitudes A_n , to the contrary, *decrease*. There is no contradiction hereat because for most of the intervals traversed the intra-channel oscillation period $2\pi\tau$ is much greater than the time of particle passage across the interval, thus the particle is far from making a full oscillation in each interval, anyway. In fact, the lower is the amplitude A_n compared to the interval length (along the particle motion direction), the stronger warp of the trajectory on this interval may occur (see Figs. 2, 3).

III. PARTICLE REFLECTION

A. Reflection conditions for positive particles

It is clear that the decrease of amplitudes (27) can not continue indefinitely, because eventually arguments of the arcsines in (28) shall exceed unity (that happens sooner than the radicand in (27) becomes negative). This merely signals that the particle can not reach the next inter-planar interval. The particle will continue the harmonic motion until it hits the previous interval, then proceeds moving outwards in the radial variable in the same but reverse way, and on the exit from the crystal it will emerge as a deflected beam.

Let us evaluate the order number $n_{\max}^{(+)}$ of the reflection interval. If for some n inequality $\frac{d}{2} + \delta \leq A_{n-1}$ is met, then it also entails $\frac{d}{2} - \delta \leq A_n$, so arguments of all the arcsines in (29) are less than unity. So, $n_{\max}^{(+)}$ is the largest integer yet allowing for $\frac{d}{2} - \delta \leq A_{n_{\max}^{(+)}}$. Through (27), that condition determines the reflection interval order number:

$$n_{\max}^{(+)} = \left\lfloor \frac{\tau^2 \theta_0^2 + (b + \delta)^2 - (\frac{d}{2} - \delta)^2}{2\delta d} \right\rfloor, \quad (30)$$

where the lower-corner brackets $\lfloor \dots \rfloor$ designate the integer part of a number ($\lfloor a \rfloor \leq a$). If $\tau\theta_0 \gg d$, variation of $n_{\max}^{(+)}(b)$ is much smaller than its mean value

$$n_{\max} \sim \frac{\tau^2 \theta_0^2}{2\delta d} = \frac{R}{2d} \theta_0^2 \quad (31)$$

(essentially valid for negative particles as well – see Eq. (51) below). It is instructive to notice that

$$\frac{d}{2} - \delta \leq A_{n_{\max}^{(+)}} < \frac{d}{2} + \delta.$$

Toward the volume reflection problem, we are interested in finding the total reflection angle θ_{ref} , half of which, by symmetry reasons, amounts to deflection angle of the trajectory in the reflection point $t = t_{\text{ref}}$ in which

$$\dot{r}(t_{\text{ref}}) = 0, \quad (32)$$

i. e.,

$$\frac{1}{2}\theta_{\text{refl}} \simeq \dot{x}(t_{\text{refl}}) = -\theta_0 + \delta \frac{t_{\text{refl}}}{\tau} \quad (33)$$

(more exactly – see Eq. (52) below) [20]. To evaluate the right-hand side of (33), one only needs to know the value of t_{refl} . The latter is found from solving equation $\dot{r}(t_{\text{refl}}) = 0$:

$$\begin{aligned} \frac{t_{\text{refl}}}{\tau} &= \frac{t_{n_{\text{max}}^{(+)}}}{\tau} + \frac{\pi}{2} \\ &= \frac{\pi}{2} + \sum_{n=1}^{n_{\text{max}}^{(+)}} \left(\arcsin \frac{\frac{d}{2} + \delta}{A_{n-1}} + \arcsin \frac{\frac{d}{2} - \delta}{A_n} \right) \\ &\quad - \arcsin \frac{b + \delta}{A_0}. \end{aligned} \quad (34)$$

The largest contribution to the emerging sum comes from the terms $n \sim n_{\text{max}}^{(+)}$ (where denominators A_n are smallest), so it may be more convenient to revert here the summation order. Introducing a useful parameter [21]

$$\nu^{(+)} = \left\{ \frac{\tau^2 \theta_0^2 + (b + \delta)^2 - \left(\frac{d}{2} - \delta\right)^2}{2\delta d} \right\}_f, \quad (35)$$

with braces $\{\dots\}_f$ to indicate the fractional part ($0 \leq \nu^{(+)} < 1$), one recasts (34) as

$$\begin{aligned} \frac{t_{\text{refl}}}{\tau} &= \frac{\pi}{2} - \arcsin \frac{b + \delta}{\sqrt{\left(\frac{d}{2} - \delta\right)^2 + 2\left(\nu^{(+)} + n_{\text{max}}^{(+)}\right)\delta d}} \\ &\quad + \sum_{n=0}^{n_{\text{max}}^{(+)}-1} \left(\arcsin \frac{\frac{d}{2} + \delta}{\sqrt{\left(\frac{d}{2} + \delta\right)^2 + 2\left(\nu^{(+)} + n\right)\delta d}} \right. \\ &\quad \left. + \arcsin \frac{\frac{d}{2} - \delta}{\sqrt{\left(\frac{d}{2} - \delta\right)^2 + 2\left(\nu^{(+)} + n\right)\delta d}} \right). \end{aligned} \quad (36a)$$

Equivalently, using the identity $\arcsin \frac{1}{\sqrt{1+\eta}} = \text{arccot} \sqrt{\eta}$, one can write

$$\begin{aligned} \frac{t_{\text{refl}}}{\tau} &= \frac{\pi}{2} - \arcsin \frac{b + \delta}{\sqrt{\left(\frac{d}{2} - \delta\right)^2 + 2\left(\nu^{(+)} + n_{\text{max}}^{(+)}\right)\delta d}} \\ &\quad + \sum_{n=0}^{n_{\text{max}}^{(+)}-1} \left(\text{arccot} \frac{\sqrt{2\left(\nu^{(+)} + n\right)\delta d}}{\frac{d}{2} + \delta} + \text{arccot} \frac{\sqrt{2\left(\nu^{(+)} + n\right)\delta d}}{\frac{d}{2} - \delta} \right). \end{aligned} \quad (36b)$$

B. Negative particles

In contrast to the trigonometric arc-sine, the hyperbolic arc-sine function exists at any value of its argument. Therefore, expression (26) for negatively charged particle trajectories holds until the radicand in the motion

amplitude A_n given by (27) becomes negative. The first interval at which that happens will be called ‘‘inflection’’ one, its order number is inferred to be

$$n_{\text{infl}} = \left\lfloor \frac{\tau^2 \theta_0^2 - (b - \delta)^2}{2\delta d} \right\rfloor + 1. \quad (37)$$

In the inflection interval the amplitude $A_{n_{\text{infl}}}$ calculated by the formula (27) would be imaginary. That implies that the $r(t)$ dependence now is to be described by a hyperbolic cosine rather than a sine (hence the term ‘‘inflection’’). Matching the amplitude and the phase of the hyperbolic cosine with solution (26) for the preceding $n = n_{\text{infl}} - 1$ gives

$$\begin{aligned} r_{n_{\text{infl}}}(t) &= -\delta - n_{\text{infl}}d + |A_{n_{\text{infl}}}| \cosh \left(\frac{t}{\tau} + \varphi_0 + \sum_{m=1}^{n_{\text{infl}}-1} \Delta \varphi_m \right. \\ &\quad \left. - \text{arsinh} \frac{\frac{d}{2} - \delta}{A_{n_{\text{infl}}-1}} - \text{arcosh} \frac{\frac{d}{2} + \delta}{|A_{n_{\text{infl}}}|} \right), \\ &\quad \left(-\frac{d}{2} - n_{\text{infl}}d \leq r_{n_{\text{infl}}} \leq \frac{d}{2} - n_{\text{infl}}d \right) \end{aligned} \quad (38)$$

where

$$\begin{aligned} |A_{n_{\text{infl}}}| &= \sqrt{-\tau^2 \theta_0^2 + (b - \delta)^2 + 2n_{\text{infl}}\delta d} \\ &\equiv \sqrt{2\delta d (1 - \nu^{(-)})}, \end{aligned} \quad (39)$$

with [22]

$$\nu^{(-)} = \left\{ \frac{\tau^2 \theta_0^2 - (b - \delta)^2}{2\delta d} \right\}_f. \quad (40)$$

Since $\frac{d}{2} + \delta \geq \sqrt{2\delta d}$, the argument of arcosh in (38) is always ≥ 1 .

Next, a question arises, at which condition the trajectory (38) can actually reach the next interval, i. e. $r_{n_{\text{infl}}}(t)$ can descend to value $n_{\text{infl}}d - \frac{d}{2}$. Since by Eq. (40), $r_{n_{\text{infl}}}(t) \geq -\delta - n_{\text{infl}}d + |A_{n_{\text{infl}}}|$, that would require

$$\delta - \frac{d}{2} > |A_{n_{\text{infl}}}|. \quad (41)$$

Substituting here (39), one may present (41) in form

$$\frac{\delta}{d} > f(\nu^{(-)}) \quad (42)$$

with

$$f(\nu^{(-)}) = \frac{3}{2} - \nu^{(-)} + \sqrt{(2 - \nu^{(-)}) (1 - \nu^{(-)})}. \quad (43)$$

Function f varies monotonously (almost linearly) in between its limiting values $f(0) = \frac{3}{2} + \sqrt{2} \approx 2.9$ and $f(1) = \frac{1}{2}$ achieved at the edges of the definition interval $[0, 1)$.

In the simplest case illustrated in Fig. 3, when condition (42) is violated (e. g. if $\delta < \frac{d}{2}$, see Fig. 3), (37)

must be the last interval reached by the particle, its order number being

$$n_{\max}^{(-)} = n_{\text{infl}} = \left\lfloor \frac{\tau^2 \theta_0^2 - (b - \delta)^2}{2\delta d} \right\rfloor + 1. \quad \left(\frac{\delta}{d} \leq f(\nu^{(-)}) \right) \quad (44)$$

Expressing t_{refl} from equation $\dot{r}(t_{\text{refl}}) = 0$ then gives

$$\begin{aligned} \frac{t_{\text{refl}}}{\tau} = & \text{arcosh} \frac{\frac{d}{2} + \delta}{|A_{n_{\text{infl}}}|} - \text{arsinh} \frac{b - \delta}{A_0} \\ & + \sum_{n=0}^{n_{\text{infl}}-1} \text{arsinh} \frac{\frac{d}{2} - \delta}{A_n} + \sum_{n=1}^{n_{\text{infl}}-1} \text{arsinh} \frac{\frac{d}{2} + \delta}{A_n}. \end{aligned} \quad (45)$$

Change of the summation order here leads to an expression

$$\begin{aligned} \frac{t_{\text{refl}}}{\tau} = & \text{arcosh} \frac{\frac{d}{2} + \delta}{\sqrt{2\delta d(1 - \nu^{(-)})}} - \text{arsinh} \frac{b - \delta}{A_0} \\ & + \sum_{n=0}^{n_{\text{infl}}-1} \text{arsinh} \frac{\frac{d}{2} - \delta}{\sqrt{2\delta d(\nu^{(-)} + n)}} \\ & + \sum_{n=0}^{n_{\text{infl}}-2} \text{arsinh} \frac{\frac{d}{2} + \delta}{\sqrt{2\delta d(\nu^{(-)} + n)}}. \end{aligned} \quad (46)$$

Therethrough, using Eq. (33) results the deflection angle.

Otherwise, i. e. if (42), is valid (e. g. if $\delta > 3d$), in all the intervals beyond (37) the trajectory must also express through hyperbolic cosines:

$$\begin{aligned} r_n(t) = & -\delta - nd + |A_n| \cosh \left(\frac{t}{\tau} + \varphi_0 + \sum_{m=1}^{n_{\text{infl}}-1} \Delta\varphi_m \right. \\ & \left. - \text{arsinh} \frac{\frac{d}{2} - \delta}{A_{n_{\text{infl}}-1}} - \text{arcosh} \frac{\frac{d}{2} + \delta}{|A_{n_{\text{infl}}}|} \right. \\ & \left. - \sum_{m=n_{\text{infl}}+1}^n \text{arcosh} \frac{\frac{d}{2} + \delta}{|A_m|} + \sum_{m=n_{\text{infl}}}^{n-1} \text{arcosh} \frac{-\frac{d}{2} + \delta}{|A_m|} \right), \quad (47) \\ & \left(-\frac{d}{2} - nd \leq r_n \leq \frac{d}{2} - nd, \quad n \geq n_{\text{infl}} \right) \end{aligned}$$

with amplitudes A_n still given by Eq. (27). Sequence (47) may continue as long as the arguments of all arcosh exceed unity, i. e. as long as

$$\frac{d}{2} + \delta \geq |A_n| \quad (48)$$

(which is equivalent to $-\frac{d}{2} + \delta \geq |A_{n-1}|$). Substituting here (27), one ultimately obtains the value of the reflection interval order number:

$$n_{\max}^{(-)} = \left\lfloor \frac{\tau^2 \theta_0^2 - (b - \delta)^2 + \left(\frac{d}{2} + \delta\right)^2}{2\delta d} \right\rfloor. \quad \left(\frac{\delta}{d} > f(\nu^{(-)}) \right) \quad (49)$$

The above expression may be compared with Eq. (30) for positively charged particles. As one might expect, in the

high-energy limit $\delta \gg d$, b values $n_{\max}^{(+)}$ and $n_{\max}^{(-)}$ coincide and do not depend on the particle energy.

Expressing t_{refl} from $\dot{r}(t_{\text{refl}}) = 0$ and Eq. (47) in this case gives

$$\begin{aligned} \frac{t_{\text{refl}}}{\tau} = & -\text{arsinh} \frac{b - \delta}{A_0} \\ & + \sum_{n=0}^{n_{\text{infl}}-1} \text{arsinh} \frac{\frac{d}{2} - \delta}{A_n} + \sum_{n=1}^{n_{\text{infl}}-1} \text{arsinh} \frac{\frac{d}{2} + \delta}{A_n}. \\ & + \sum_{m=n_{\text{infl}}}^{n_{\max}^{(-)}} \text{arcosh} \frac{\frac{d}{2} + \delta}{|A_m|} \\ & - \sum_{m=n_{\text{infl}}}^{n_{\max}^{(-)}-1} \text{arcosh} \frac{-\frac{d}{2} + \delta}{|A_m|} \\ \equiv & -\text{arsinh} \frac{b - \delta}{\sqrt{2\delta d(n_{\text{infl}} - 1 + \nu^{(-)})}} \\ & + \sum_{n=0}^{n_{\text{infl}}-1} \text{arsinh} \frac{\frac{d}{2} - \delta}{\sqrt{2\delta d(\nu^{(-)} + n)}} \\ & + \sum_{n=0}^{n_{\text{infl}}-2} \text{arsinh} \frac{\frac{d}{2} + \delta}{\sqrt{2\delta d(\nu^{(-)} + n)}}, \\ & + \sum_{n=1}^{n_{\max}^{(-)}-n_{\text{infl}}+1} \text{arcosh} \frac{\frac{d}{2} + \delta}{\sqrt{2\delta d(n - \nu^{(-)})}} \\ & - \sum_{n=1}^{n_{\max}^{(-)}-n_{\text{infl}}} \text{arcosh} \frac{-\frac{d}{2} + \delta}{\sqrt{2\delta d(n - \nu^{(-)})}}. \end{aligned} \quad (50)$$

Actually, equations (50) can be used not only under condition (42), but also at any ratio $\frac{\delta}{d}$, provided in capacity of $n_{\max}^{(-)}$ one uses the expression

$$n_{\max}^{(-)} = \left\lfloor \frac{\tau^2 \theta_0^2 - (b - \delta)^2 + \left(\frac{d}{2} - \delta\right)^2 \Theta\left(\frac{\delta}{d} - f(\nu^{(-)})\right)}{2\delta d} \right\rfloor + 1 \quad (51)$$

(with $\Theta(v)$ the Heavyside unit-step function) unifying (44) and (49). Such a universal approach is most convenient at evaluation of t_{refl} with the aid of computer.

The obtained expressions (26-29) for the trajectory and (36, 50) for its reflection point allow evaluating all the observables relevant to the particle passage. In the present paper, we will be interested only in the final angle of elastic reflection.

C. Thick crystal limit (isolation of volume effects)

Formulas (36, 50), in principle, contain dependencies both on volume and on initial and boundary effects. In most practical cases, the deflecting crystal may be regarded as thick, whence boundary effects are expected

to become negligible. An increase of the crystal thickness, or more precisely of the distance between the crystal boundary and the volume reflection point, may be thought of as an increase of the particle incidence angle θ_0 (see Fig. 1). Then, it suffices to consider the limit

$$\theta_{\text{refl}} \approx \theta_{\text{v.r.}} = 2 \lim_{\theta_0/\theta_c \rightarrow \infty} \left(-\theta_0 + \delta \frac{t_{\text{refl}}(\theta_0)}{\tau^2} \right). \quad (52)$$

With function (36), or (50), such a limit must always be finite: indeed, at large n_{max} the sum over n grows like the corresponding integral, whose asymptotic behavior straightforwardly evaluates as

$$\begin{aligned} \frac{t_{\text{refl}}}{\tau} &\sim \int^{n_{\text{max}}} dn \left(\frac{\frac{d}{2} + \delta}{\sqrt{2(\nu^{(+)} + n)\delta d}} + \frac{\frac{d}{2} - \delta}{\sqrt{2(\nu^{(+)} + n)\delta d}} \right) \\ &\sim \sqrt{\frac{2n_{\text{max}}d}{\delta}} \simeq \theta_0 \frac{\tau}{\delta}. \end{aligned}$$

This leading asymptotic behavior cancels exactly the first term in (52), whilst calculation of the finite remainder requires a more accurate estimation of the sum, which will be our task in the next section (in application to the limit $R \gg R_c$).

In general, it must be noted that function $\theta_{\text{v.r.}}(\tau, \delta, d, b)$, being a dimensionless function of 4 dimensional variables, may depend only on their 3 dimensionless ratios: say, d/τ , δ/d , b/d . At that, the last ratio is always ~ 1 . The first one amounts to

$$\frac{d}{\tau} = \sqrt{\frac{2d}{R_c}} = 2\theta_c, \quad (53)$$

where θ_c is the Lindhard critical angle [7]; so, it is always small, once we are in a high-energy regime. As for the ratio

$$\frac{2\delta}{d} = \frac{R_c}{R}, \quad (54)$$

it may be either large or small depending on the particle energy and the crystal bending radius. The regime of particle passage through the crystal is determined solely by ratio (54).

At $R \sim R_c$ formulas (36, 50) allow for no further appreciable simplification, but as they are, they are sufficiently well suited for numerical calculations. Fig. 4 shows the evaluated dependence of the volume reflection angle on the impact parameter, for positive and negative particles. Many of the features observed allow for a straightforward qualitative explanation.

1. The origin of the recurrent structure in variable b with a tapering period is, obviously, due to $\theta_{\text{v.r.}}$ dependence on b through $\nu^{(\pm)}$ alone (see Eqs. (35), (40)), insofar as $\nu^{(\pm)}$, involving an operation of fractional part, is a periodic function of $\frac{(b \pm \delta)^2}{2\delta d}$, which in the interval $-\frac{d}{2} < b < \frac{d}{2}$ makes $\sim 2\frac{d^2}{8\delta d} =$

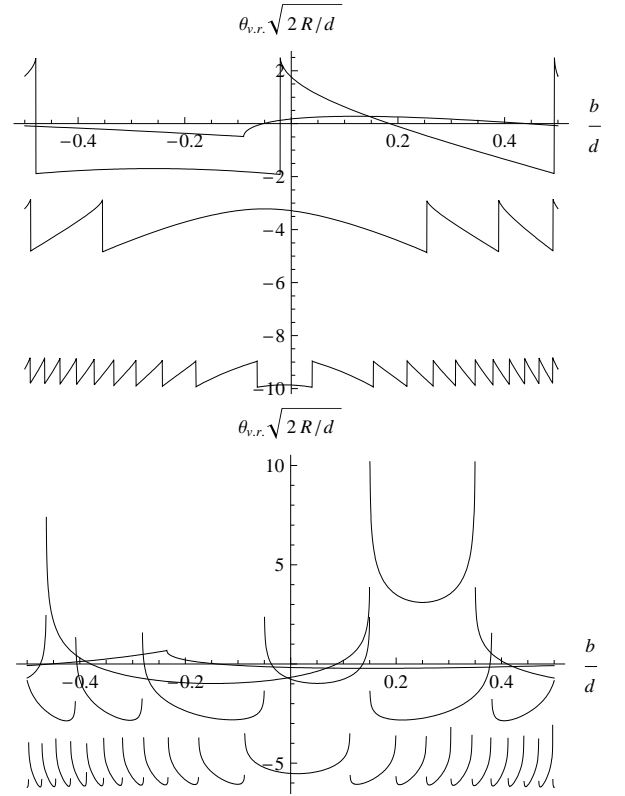


FIG. 4: The volume reflection angle $\theta_{\text{v.r.}}$ as a function of impact parameter b , for $R/R_c = 1/3, 2, 10, 40$. Top panel – for positively charged particles, bottom panel – for negatively charged particles. Beyond the shown unit interval the picture repeats periodically.

$\frac{R}{2R_c} \gg 1$ periods. Also, since $\nu^{(\pm)}$ is an even function of $b \pm \delta$, the particle deflection angle is a symmetric function of b with respect to point $b = -\delta$ for positively charged particles, and with respect to $b = \delta$ for negative particles.

2. Another feature of $\theta_{\text{v.r.}}(b)$ dependence(s) is that, for negatively charged particles, the reflection angle blows up (formally) to $+\infty$ at certain values of impact parameters. Physically, that corresponds to close matching of the particle transverse energy to the height of a (locally parabolic) effective potential barrier – the situation known as orbiting (see [8]). Its significance within the problem of negative particle volume reflection was advocated in [9]. The asymptotics of the divergences is logarithmic [8], as follows from the general integral expression of the

deflection angle in a central potential $V(r)$ [23]:

$$\theta \underset{E \gg m}{\approx} 2M \int_{r_{\min}}^{\infty} \frac{dr/(R+r)^2}{\sqrt{(E-V(r))^2 - M^2/(R+r)^2}} - \pi \quad (55a)$$

$$R \gg r, b \quad \frac{1}{R} \int_{r_{\min}}^{\infty} \frac{dr}{\sqrt{\frac{b}{2R} - \frac{V_{\text{eff}}(r)}{2E}}} - \pi \quad (55b)$$

$$\underset{\text{orbit.}}{\sim} \theta_c \frac{4\delta}{d} \int_{|r-r_{\text{saddle}}| \lesssim d} \frac{dr}{\sqrt{2\delta\Delta b + (r-r_{\text{saddle}})^2}} + \dots \quad (55c)$$

$$\underset{\sim}{\approx} \theta_c \frac{4\delta}{d} \begin{cases} \ln \frac{d^2}{2\delta\Delta b} + \dots & \Delta b > 0 \\ \frac{1}{2} \ln \frac{d^2}{2\delta|\Delta b|} + \dots & \Delta b < 0. \end{cases} \quad (55d)$$

Here $M = E(R - b)$ is the particle angular momentum relative to the crystal bend axis, $V_{\text{eff}}(r) = V(r) - E\frac{r}{R}$ – the effective potential including the centrifugal energy, r_{saddle} – the position of maximum of the effective potential barrier whose height in the case of orbiting happens to be close to the particle energy, and Δb – the particle impact parameter variation relative to the value at which the particle energy exactly equals to the height of the effective potential barrier. The factor $\frac{1}{2}$ in the $\Delta b < 0$ case of Eq. (55d) arises because the integration in (55c) is then carried out only over the one-sided neighborhood of r_{saddle} where the radicand stays positive (see Fig. 5).

3. It must also be noticed that function $\theta_{v.r.}(b)$ for negative particles has smooth minima, which must correspond to caustics, i. e., to rainbow scattering [8].
4. In contrast, for positive particles the potential in its maximum is not differentiable, thus there is neither orbiting, nor rainbow scattering in this case.

IV. VOLUME REFLECTION REGIME (MODERATELY HIGH ENERGIES, $R \gg R_c$)

As we had mentioned in the Introduction, and as Fig. 4 does confirm, the pattern of stable (virtually impact parameter independent) particle deflection, originally named volume reflection, emerges under the condition $R \gg R_c$, i. e. $2\delta \ll d$. In the given, practically interesting limit the generic formulas for the particle deflection angle can be substantially simplified, which will be our aim in this section. The treatment is somewhat different for the cases of positively and negatively charged particles, because of the difference between the functional form of initial Eqs. (36) and (50).

A. Positive particles

For positively charged particles, in the considered limiting case $\delta \ll d$, it is possible to replace the sum-

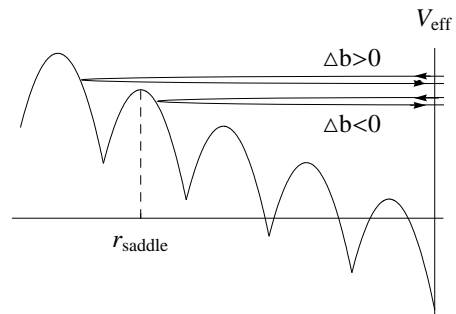


FIG. 5: The relation between the particle radial energy and the effective potential energy V_{eff} (including the centrifugal potential) under the conditions of negative charged particle orbiting in a bent crystal. The leading logarithmic contribution to integral (55b) comes from the vicinity of point r_{saddle} – the coordinate of the effective potential maximum to which the particle radial energy happens to be close. In the case $\Delta b > 0$ the particle sweeps the two-sided neighborhood of r_{saddle} , whereas at $\Delta b < 0$ – its one-sided neighborhood only.

mation in (36) by integration, because, say, quantity $(\frac{d}{2} \pm \delta)^2 + 2(\nu^{(+)} + n)\delta d$ entering the denominators in (36a) varies relatively little as n changes from n to $n+1$. The proper mathematical tool for approximating sums by integrals is the Euler-Maclaurin formula (see, e. g., [11]) which reads

$$\sum_{n=0}^N f(n) = \int_0^N dn f(n) + \frac{1}{2}f(0) + \frac{1}{2}f(N) + \mathcal{O}\left(\frac{df}{dn}\right). \quad (56)$$

Employing this formula for approximation of each of the sums in (36b) (which is somewhat more convenient than Eq. (36a)), one gets [24]

$$\begin{aligned} & \sum_{n=0}^{n_{\max}^{(+)}-1} \text{arccot} \frac{\sqrt{2\delta d(\nu^{(+)} + n)}}{\frac{d}{2} \pm \delta} \\ &= \int_{\nu^{(+)}}^{n_{\max}^{(+)} + \nu^{(+)} - 1} dn \text{arccot} \frac{\sqrt{2\delta dn}}{\frac{d}{2} \pm \delta} \\ &+ \frac{1}{2} \text{arccot} \frac{\sqrt{2\delta d\nu^{(+)}}}{\frac{d}{2} \pm \delta} + \frac{1}{2} \text{arccot} \frac{\sqrt{2\delta d(n_{\max}^{(+)} + \nu^{(+)} - 1)}}{\frac{d}{2} \pm \delta} \\ &+ \mathcal{O}\left(\sqrt{\frac{\delta}{d}}\right), \quad (57) \end{aligned}$$

where we had estimated, for all n ,

$$\left| \frac{d}{dn} \text{arccot} \frac{\sqrt{2\delta d(\nu^{(+)} + n)}}{\frac{d}{2} \pm \delta} \right| \lesssim \sqrt{\frac{\delta}{d}}. \quad (58)$$

The two end-point contributions in the third line of (57) are small as $\mathcal{O}(\delta/d)$ relative to the integral, but still they need to be kept if we wish to describe not only the mean deflection, but also the scattered beam shape.

Taking the indefinite integral in Eq. (57) by parts

$$\int dn \operatorname{arccot} \sqrt{an} = \frac{1}{a} [(1+an) \operatorname{arccot} \sqrt{an} + \sqrt{an}],$$

one brings (57) to the form

$$\begin{aligned} & \sum_{n=0}^{n_{\max}^{(+)}-1} \operatorname{arccot} \frac{\sqrt{2\delta d(\nu^{(+)}+n)}}{\frac{d}{2} \pm \delta} \\ & \stackrel{\delta \ll d}{\approx} \frac{(\frac{d}{2} \pm \delta)^2}{2\delta d} \left(\left[1 + \frac{2\delta d}{(\frac{d}{2} \pm \delta)^2} (n_{\max}^{(+)} + \nu^{(+)} - 1) \right] \right. \\ & \quad \cdot \operatorname{arccot} \frac{\sqrt{2\delta d(n_{\max}^{(+)} + \nu^{(+)} - 1)}}{\frac{d}{2} \pm \delta} \\ & \quad + \frac{\sqrt{2\delta d(n_{\max}^{(+)} + \nu^{(+)} - 1)}}{\frac{d}{2} \pm \delta} \\ & \quad - \left[1 + \frac{2\delta d\nu^{(+)}}{(\frac{d}{2} \pm \delta)^2} \right] \operatorname{arccot} \frac{\sqrt{2\delta d\nu^{(+)}}}{\frac{d}{2} \pm \delta} - \frac{\sqrt{2\delta d\nu^{(+)}}}{\frac{d}{2} \pm \delta} \\ & \quad + \frac{1}{2} \operatorname{arccot} \frac{\sqrt{2\delta d\nu^{(+)}}}{\frac{d}{2} \pm \delta} + \frac{1}{2} \operatorname{arccot} \frac{\sqrt{2\delta d(n_{\max}^{(+)} + \nu^{(+)} - 1)}}{\frac{d}{2} \pm \delta} \\ & \quad \left. + \mathcal{O}\left(\sqrt{\frac{\delta}{d}}\right) \right). \quad (59) \end{aligned}$$

In the limit $n_{\max}^{(+)} \rightarrow \infty$, with the use of asymptotic expansion $\operatorname{arccot} \sqrt{\eta} = \frac{\pi}{2} - \sqrt{\eta} + \mathcal{O}(\eta^{3/2})$, expression (59) reduces to

$$\begin{aligned} & \sum_{n=0}^{n_{\max}^{(+)}-1} \operatorname{arccot} \frac{\sqrt{2\delta d(\nu^{(+)}+n)}}{\frac{d}{2} \pm \delta} \\ & \xrightarrow{n_{\max}^{(+)} \gg 1} \frac{d \pm 2\delta}{\sqrt{2\delta d}} \sqrt{n_{\max}^{(+)}} \\ & - \frac{(\frac{d}{2} \pm \delta)^2}{2\delta d} \left[\left(1 + \frac{2\delta d}{(\frac{d}{2} \pm \delta)^2} \right) \left(\frac{\pi}{2} - \frac{\sqrt{2\delta d\nu^{(+)}}}{\frac{d}{2} \pm \delta} \right) + \frac{\sqrt{2\delta d\nu^{(+)}}}{\frac{d}{2} \pm \delta} \right] \\ & + \frac{1}{2} \cdot \frac{\pi}{2} + \mathcal{O}\left(\frac{1}{\sqrt{n_{\max}^{(+)}}}, \sqrt{\frac{\delta}{d}}\right). \quad (60) \end{aligned}$$

Here, one notices that terms $-\frac{\sqrt{2\delta d\nu^{(+)}}}{\frac{d}{2} \pm \delta}$, $+\frac{\sqrt{2\delta d\nu^{(+)}}}{\frac{d}{2} \pm \delta}$ in the brackets in (60) cancel out. Further on, substituting (60) to (36b) and this to (52), we witness the anticipated cancellation of the large terms $-\theta_0 + \frac{\sqrt{2\delta d}}{\tau} n_{\max}^{(+)} \cong 0$, and

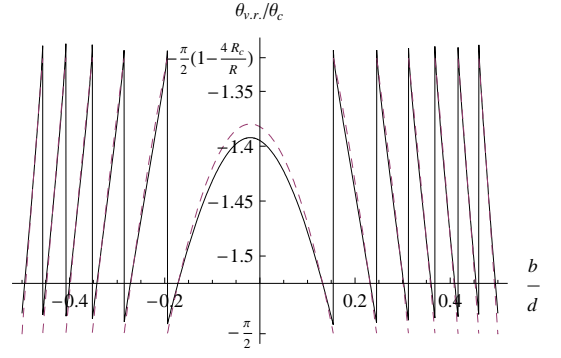


FIG. 6: Solid curve – positively charged particle reflection angle $\theta_{v.r.}$ versus impact parameter b , for $R/R_c = 25$. Dashed curve – approximation (61). The central segment of the curves is strongly θ_0 -dependent.

ultimately arrive at a finite result:

$$\begin{aligned} \theta_{v.r.}(b) & \approx -2\theta_0 + 2\frac{\delta}{\tau} \left(\frac{\pi}{2} + \frac{2d}{\sqrt{2\delta d}} \sqrt{n_{\max}^{(+)}} \right. \\ & \quad - \frac{\pi}{2} \left[\frac{(\frac{d}{2} + \delta)^2}{2\delta d} + \nu^{(+)} \right] + \frac{\pi}{4} \\ & \quad \left. - \frac{\pi}{2} \left[\frac{(\frac{d}{2} - \delta)^2}{2\delta d} + \nu^{(+)} \right] + \frac{\pi}{4} \right) \\ & \equiv -\frac{\pi}{2} \theta_c \left[1 + \frac{4R_c}{R} (\nu^{(+)}(b) - 1) + \mathcal{O}\left(\frac{R_c^{3/2}}{R^{3/2}}\right) \right] \quad (61) \end{aligned}$$

(with $\nu^{(+)}(b)$ being given by Eq. (35)).

Comparison of the approximation (61) with the exact result (36) is shown in Fig. 6. (Actually, the given approximation appears to be numerically accurate starting from $R/R_c \sim 5$). From the figure (or Eq. (61)) one concludes that in the first approximation all the particles are deflected to the same angle $\approx -\frac{\pi}{2}\theta_c$. There is also some dispersal of the scattering angles, depending on the particle impact parameter, of the full width

$$\Delta\theta_{v.r.} = \theta_c \frac{2\pi R_c}{R} \equiv \frac{2\pi\delta}{\tau}. \quad (\text{pos. char. part.}) \quad (62)$$

At practice, however, the angular distribution of final particles is described not by the indicatrix $\theta_{v.r.}(b)$ but the scattering differential cross-section as a function of the scattering angle $\theta_{v.r.}$. Therefore, it is desirable to evaluate the latter dependence issuing from the first.

Differential cross-section. Turning to evaluation of the differential cross-section, one encounters a certain complication: the b -dependent quantity $\nu^{(+)}$ in (61) also contains dependence on θ_0 . Physically, that corresponds to a residual sensitivity to the boundary conditions, impairing our initial assumption about the boundary condition vanishing influence in the limit of large θ_0/θ_c . We

can not revoke it at the present stage, since in equation (52) we had already incorporated the facilitating assumption of the trajectory symmetry with respect to point t_{ref} . Obviously, the sensitivity to the boundary conditions in general destroys such a symmetry. Furthermore, θ_{ref} might as well contain a dependence on the particle *exit angle* relative to the atomic planes, which we did not even take trouble to specify. Altogether, that may rise a suspicion that the b -dependent correction obtained in (61) is unreliable for evaluating the differential cross-section. Fortunately, the impediment is not fatal and can be overcome within the present framework. As we will show, the differential cross-section sensitivity to θ_0 is weak, and furthermore, upon averaging over a tiny interval of θ_0 that dependence can be eliminated completely.

To begin with, the differential cross-section involves only a *derivative* of function $\theta_{\text{v.r.}}(b)$:

$$\begin{aligned} \frac{d\lambda}{d\theta_{\text{v.r.}}} &= \sum_m \frac{1}{|d\theta_{\text{v.r.}}/db|_{b=b_m(\theta_{\text{v.r.}})}} \\ &\equiv \frac{R}{2\pi\theta_c R_c} \sum_m \frac{1}{|d\nu^{(+)}(b)/db|_{b=b_m(\nu^{+})(\theta_{\text{v.r.}})}}, \end{aligned} \quad (63)$$

where $b_m(\theta)$ is the set of all the roots of equation $\theta_{\text{v.r.}}(b) = \theta$ belonging to the interval $-\frac{d}{2} < b < \frac{d}{2}$. Now, at $R/R_c \gg 1$ the number of roots b_m to equation $\theta_{\text{v.r.}} = \theta$ is large, and so, in general, they are densely distributed over the finite definition interval $-\frac{d}{2} < b < \frac{d}{2}$. It appears that the root distribution density is just proportional to the derivative in the denominator of (63) (the formal demonstration is relegated to the Appendix). Therefore, the sum appearing in (63) approximately equals to just the b variation interval length, i. e. d . However, the relation expected thereby,

$$\frac{d\lambda}{d\theta_{\text{v.r.}}} \simeq \frac{Rd}{2\pi\theta_c R_c}, \quad (64)$$

does not hold *uniformly* in b , and hence in $\theta_{\text{v.r.}}$. For instance, in a neighborhood of point $b = -\delta$ we have in the denominator of (63) $\partial\nu^{(+)}(b)/\partial b \rightarrow 0$ (see Fig. 6), so thereat the differential cross-section blows up above the plateau (64) (see Appendix). But the latter peak position on the $\theta_{\text{v.r.}}$ axis depends sharply on the value of θ_0 and hence is utterly *casual*, needing averaging over.

Indeed, one notes that the dependence of $\nu^{(+)}$ on θ_0 is quadratic, so a situation is possible when the incident particle beam angular divergence is smaller than the spread acquired in the crystal:

$$\Delta\theta_0 \ll \Delta\theta_{\text{v.r.}}, \quad (65)$$

but at the same time, the indeterminance of $\frac{\tau^2\theta_0^2}{2\delta d} \approx n_{\text{max}}^{(+)}$ is larger than unity:

$$\Delta \left(\frac{\tau^2\theta_0^2}{2\delta d} \right) = \frac{\tau^2\theta_0}{\delta d} \Delta\theta_0 \gg 1. \quad (66)$$

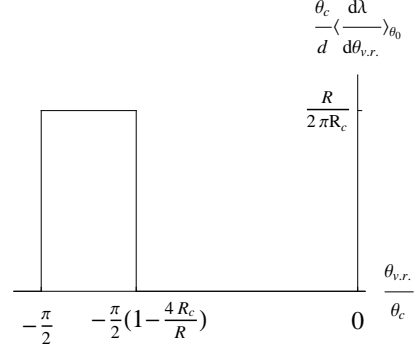


FIG. 7: Asymptotic (at $R \gg R_c$) behavior of the θ_0 -averaged differential cross-section for positively charged particle scattering (Eq. (69)). The area under the curve is unity, as the total probability. In higher orders in R_c/R the distribution edges must smear out.

Together, Eqs. (65, 66) may be viewed as a double inequality

$$\frac{2\delta\theta_c}{\tau\theta_0} \ll \Delta\theta_0 \ll \frac{2\pi\delta}{\tau}. \quad (\theta_0\text{-averaging}) \quad (67)$$

Here the gap exists provided

$$\theta_0 \gg \frac{\theta_c}{\pi}. \quad (68)$$

This is basically the same condition that we had assumed in writing Eq. (52), thus for derivation of a θ_0 -averaged differential cross-section we can safely rely on Eq. (61).

Ultimately, we can make a specific statement that under conditions (67) the θ_0 -averaged differential cross-section equals

$$\begin{aligned} \left\langle \frac{d\lambda}{d\theta_{\text{v.r.}}} \right\rangle_{\theta_0} &\approx \frac{Rd}{2\pi\theta_c R_c} \\ &\cdot \Theta\left(\theta_{\text{v.r.}} + \frac{\pi}{2}\theta_c\right) \Theta\left(-\theta_{\text{v.r.}} - \frac{\pi}{2}\theta_c\left(1 - \frac{4R_c}{R}\right)\right) \end{aligned} \quad (69)$$

(see Fig. 7).

B. Negative particles

In the case of negative particles, the starting point is Eq. (46) (relevant under (strong) condition (42)), and again, it has to be examined with the object to trade the sum for an integral. First of all, it has to be minded that at $n \sim 1$ the hyperbolic arcsine arguments vary significantly, but at the same time they are large, whereas hyperbolic arcsine of a large argument is close to logarithm of a large argument: $\text{arsinh } v \underset{v \gg 1}{\simeq} \ln 2v$, and thus varies relatively little. On the other hand, in the domain of large n the arguments of the arcsines vary little. Therefore, over the *entire* summation interval both sums involved may be approximated via integrals. Yet,

first terms in the sums are singular functions of $\nu^{(-)}$, and therefore are better taken into account separately. Thereby, application of the Euler-Maclaurin formula to the first of the sums in Eq. (46) gives

$$\begin{aligned} & \sum_{n=0}^{n_{\text{infl}}-1} \operatorname{arsinh} \frac{\frac{d}{2} - \delta}{\sqrt{2\delta d(\nu^{(-)} + n)}} \\ & \approx \ln \frac{d-2\delta}{\sqrt{2\delta d\nu^{(-)}}} + \int_{\nu^{(-)+1}^{\nu^{(-)}+n_{\text{infl}}-1}} dn \operatorname{arsinh} \frac{\frac{d}{2} - \delta}{\sqrt{2\delta d\sqrt{n}}} \\ & + \frac{1}{2} \ln \frac{d-2\delta}{\sqrt{2\delta d(\nu^{(-)}+1)}} + \frac{1}{2} \operatorname{arsinh} \frac{\frac{d}{2} - \delta}{\sqrt{2\delta d(\nu^{(-)}+n_{\text{infl}}-1)}}. \end{aligned} \quad (70)$$

The next-to-leading order (derivative-related) correction term [11] to (70) amounts

$$\frac{1}{12} \frac{d}{dn} \operatorname{arsinh} \frac{\frac{d}{2} - \delta}{\sqrt{2\delta d(\nu^{(-)} + n)}} \Big|_{n=1}^{n=n_{\text{infl}}-1} \approx -\frac{1}{24(1+\nu^{(-)})}. \quad (71)$$

We will omit it because of the smallness of the numerical coefficient $\frac{1}{24}$, although, in principle, asymptotically it is also relevant (the same is true for all the higher derivatives, whose contributions enter with yet smaller coefficients (involving inverse factorial and Bernoulli numbers)).

Next, calculating the indefinite integral in Eq. (70) by parts,

$$\int dn \operatorname{arsinh} \frac{a}{\sqrt{n}} = n \operatorname{arsinh} \frac{a}{\sqrt{n}} + a\sqrt{a^2 + n}, \quad (72)$$

we bring (70) to the form

$$\begin{aligned} & \sum_{n=0}^{n_{\text{infl}}-1} \operatorname{arsinh} \frac{\frac{d}{2} - \delta}{\sqrt{2\delta d\sqrt{\nu^{(-)} + n}}} \\ & \approx (\nu^{(-)} + n_{\text{infl}} - 1) \operatorname{arsinh} \frac{\frac{d}{2} - \delta}{\sqrt{2\delta d(\nu^{(-)} + n_{\text{infl}} - 1)}} \\ & + \frac{\frac{d}{2} - \delta}{\sqrt{2\delta d}} \sqrt{\frac{(\frac{d}{2} - \delta)^2}{2\delta d} + \nu^{(-)} + n_{\text{infl}} - 1} \\ & - (1 + \nu^{(-)}) \operatorname{arsinh} \frac{\frac{d}{2} - \delta}{\sqrt{2\delta d(1 + \nu^{(-)})}} \\ & - \frac{\frac{d}{2} - \delta}{\sqrt{2\delta d}} \sqrt{\frac{(\frac{d}{2} - \delta)^2}{2\delta d} + 1 + \nu^{(-)}} + \ln \frac{d-2\delta}{\sqrt{2\delta d\nu^{(-)}}} \\ & + \frac{1}{2} \ln \frac{d-2\delta}{\sqrt{2\delta d(1 + \nu^{(-)})}} + \frac{1}{2} \operatorname{arsinh} \frac{\frac{d}{2} - \delta}{\sqrt{2\delta d(\nu^{(-)} + n_{\text{infl}} - 1)}}. \end{aligned} \quad (73)$$

Now, in the thick-crystal limit $n_{\text{infl}} \rightarrow \infty$, Eq. (73)

simplifies to

$$\begin{aligned} & \sum_{n=0}^{n_{\text{infl}}-1} \operatorname{arsinh} \frac{\frac{d}{2} - \delta}{\sqrt{2\delta d\sqrt{\nu^{(-)} + n}}} \\ & \xrightarrow{n_{\text{infl}} \gg 1} \sqrt{n_{\text{infl}}} \frac{d-2\delta}{\sqrt{2\delta d}} - (1 + \nu^{(-)}) \ln \frac{d-2\delta}{\sqrt{2\delta d(1 + \nu^{(-)})}} \\ & - \frac{(\frac{d}{2} - \delta)^2}{2\delta d} \sqrt{1 + \frac{2\delta d}{(\frac{d}{2} - \delta)^2} (1 + \nu^{(-)})} + \ln \frac{d-2\delta}{\sqrt{2\delta d\nu^{(-)}}} \\ & + \frac{1}{2} \ln \frac{d-2\delta}{\sqrt{2\delta d(1 + \nu^{(-)})}} \\ & \cong \sqrt{n_{\text{infl}}} \frac{d-2\delta}{\sqrt{2\delta d}} - \left(\frac{1}{2} + \nu^{(-)}\right) \ln \frac{d-2\delta}{\sqrt{2\delta d(1 + \nu^{(-)})}} \\ & - \frac{(\frac{d}{2} - \delta)^2}{2\delta d} - \frac{1}{2}(1 + \nu^{(-)}) + \ln \frac{d-2\delta}{\sqrt{2\delta d\nu^{(-)}}}. \end{aligned} \quad (74)$$

Similarly, the second term in (46) reduces to

$$\begin{aligned} & \sum_{n=0}^{n_{\text{infl}}-2} \operatorname{arsinh} \frac{\frac{d}{2} + \delta}{\sqrt{2\delta d(\nu^{(-)} + n)}} \\ & \rightarrow \sqrt{n_{\text{infl}}} \frac{d+2\delta}{\sqrt{2\delta d}} - \left(\frac{1}{2} + \nu^{(-)}\right) \ln \frac{d+2\delta}{\sqrt{2\delta d(1 + \nu^{(-)})}} \\ & - \frac{(\frac{d}{2} + \delta)^2}{2\delta d} - \frac{1}{2}(1 + \nu^{(-)}) + \ln \frac{d+2\delta}{\sqrt{2\delta d\nu^{(-)}}}. \end{aligned} \quad (75)$$

Inserting (74) and (75) to Eqs. (46) and thereupon to (52), after a simple rearrangement one is left with the final result

$$\begin{aligned} \theta_{\text{v.r.}} \approx & -\theta_c \left[1 - \frac{2R_c}{R} \left(\frac{1}{2} \ln \frac{1}{e(1 - \nu^{(-)})} + \ln \frac{1}{\nu^{(-)}} \right. \right. \\ & \left. \left. - \left(\nu^{(-)} + \frac{1}{2} \right) \ln \frac{e}{(1 + \nu^{(-)})} + (1 - \nu^{(-)}) \ln \frac{R}{R_c} \right) \right] \end{aligned} \quad (76)$$

(we remind that $\nu^{(-)}(b)$ is given by Eq. (40)). Note that logarithmic asymptotics of this expression at $\nu^{(-)} \rightarrow 0$ and at $\nu^{(-)} \rightarrow 1$ agrees with the general law (55d).

The exact (52) vs. approximate (76) expressions for the indicatrix are compared in Fig. 8.

1. Differential cross-section

To deduce the observable differential cross-section from the available indicatrix $\theta_{\text{v.r.}}(\nu^{(-)}(b))$, we have again to issue from Eq. (63). To some extent, the same procedure as for positively charged particles applies here, leading to

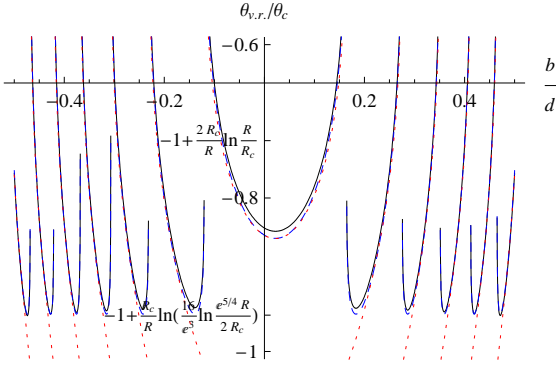


FIG. 8: Comparison of the exact formula (52, 46) (black solid curve) with the approximation (76) (blue dashed curve) and approximations (86) (red dotted curve) for $R/R_c = 25$. The central segment of the curves is strongly θ_0 -dependent.

representation

$$\frac{d\lambda}{d\theta_{v.r.}} = \sum_{j=1}^2 \left| \frac{d\nu^{(-)}}{d\theta_{v.r.}} \right| \sum_m \frac{1}{|\partial \nu_j^{(-)}/\partial b|} \Big|_{b=b_m(\nu_j^{(-)}(\theta_{v.r.}))}, \quad (77)$$

where $b_m(\nu^{(-)})$ is the solution of Eq. (40), $\sum_{j=1}^2$ accounts for the existence of two roots for equation $\theta_{v.r.} = \theta_{v.r.}(\nu^{(-)})$ with the function (76). Again, upon averaging over θ_0 under condition (67) (cf. Appendix), one obtains:

$$\frac{1}{d} \left\langle \frac{d\lambda}{d\theta_{v.r.}} \right\rangle_{\theta_0} = \sum_{j=1}^2 \left| \frac{d\nu_j^{(-)}}{d\theta_{v.r.}} \right|. \quad (78)$$

Let us recall the interpretation familiar from the positive particle case, that after the averaging over θ_0 parameter $\nu^{(-)}$, just like the parameter b/d , becomes a uniformly distributed random quantity in a unit variation interval. For each given b , and thus $\theta_{v.r.}$, one can always unambiguously tell whether $\nu^{(-)} = \nu_1^{(-)}$ or $\nu^{(-)} = \nu_2^{(-)}$, so the probability normalization is conserved under conditions of summation over the branches.

A technical distinction of the case with negative particles is that equation (76) can *not* be resolved with respect to $\nu^{(-)}$ in an explicit and exact form. Of course, it can be solved numerically; the differential cross-section so evaluated is shown in Fig. 9, by a solid curve. On the other hand, it is also useful to pursue an analytic but approximate approach, based on different approximations in different regions of $\nu^{(-)}$, which will be our last effort.

2. Approximate solution for $\nu^{(-)}(\theta_{v.r.})$.

In Eq. (76) at typical $\nu^{(-)}$ the leading term is the last one, where $\nu^{(-)}$ is multiplied by a large logarithm. Besides that, in the domain of $\nu^{(-)}$ close to 1 the first logarithm in (76) becomes large, too, and a minimum of

function $\theta_{v.r.}(\nu^{(-)})$ develops, corresponding to onset of a rainbow scattering. As for the second logarithm in (76), which raises at $\nu^{(-)} \rightarrow 0$, it does not lead to formation of a dependence $\theta_{v.r.}(\nu^{(-)})$ minimum – on the contrary, it makes the dependence steeper, and in the area of its significance the differential cross-section is small (exponentially). So, for the differential cross-section description it basically suffices to consider only two regions: the region where the last term of (76) dominates, and the region where the last term and $\frac{1}{2} \ln \frac{1}{e(1-\nu^{(-)})}$ in (76) are competing. On the $\theta_{v.r.}$ axis the mentioned regions are adjacent, and conjointly they should give almost the full picture of the differential cross-section variation. For completeness, one may consider also a third, asymptotic region of the the differential cross-section tail (orbiting region), where the first and the second logarithms of (76) dominate.

a. *Rainbow region.* The value of $\nu^{(-)}$ corresponding to the rainbow angle is to be determined from condition

$$\frac{\partial \theta_{v.r.}}{\partial \nu^{(-)}} \Big|_{\nu^{(-)}=\nu_0^{(-)}} = 0, \quad (79)$$

which in application to expression (76) gives

$$\frac{\nu_0^{(-)}}{1-\nu_0^{(-)2}} - \frac{1}{\nu_0^{(-)}} + \ln(1+\nu_0^{(-)}) = \ln \frac{R}{R_c} \gg 1. \quad (80)$$

The approximate solution of Eq. (80) is

$$\nu_0^{(-)} \approx 1 - \frac{1}{2 \ln \frac{e^{5/4} R}{2R_c}} + \mathcal{O}\left(\frac{1}{\ln^3 \frac{e^{5/4} R}{2R_c}}\right). \quad (81)$$

In vicinity of the found point $\nu_0^{(-)}$ we may expand function $\theta_{v.r.}(\nu^{(-)})$ up to a quadratic term

$$\begin{aligned} \left(\frac{\theta_{v.r.}}{\theta_c} + 1\right) \frac{R}{2R_c} &\approx \frac{1}{2} \ln \left(\frac{16}{e^3} \ln \frac{e^{5/4} R}{2R_c}\right) \\ &+ (\nu^{(-)} - \nu_0^{(-)})^2 \ln^2 \frac{e^{5/4} R}{2R_c} \\ &+ \mathcal{O}\left((\nu^{(-)} - \nu_0^{(-)})^3 \ln^3 \frac{e^{5/4} R}{2R_c}\right). \end{aligned} \quad (82)$$

Now, expressing the pair of roots $\nu_j^{(-)}(\theta_{v.r.})$ from the quadratic equation (82), one derives by formula (77) the behavior of the θ_0 -averaged differential cross-section in vicinity of the rainbow angle:

$$\frac{\theta_c}{d} \left\langle \frac{d\lambda}{d\theta_{v.r.}} \right\rangle_{\theta_0} \approx \frac{\sqrt{R/2R_c}}{\ln \frac{e^{5/4} R}{2R_c} \sqrt{\frac{\theta_{v.r.}}{\theta_c} + 1 - \frac{R_c}{R} \ln \left(\frac{16}{e^3} \ln \frac{e^{5/4} R}{2R_c}\right)}}. \quad (83)$$

The domain of applicability of this approximation is determined from Eq. (82) by demanding the third-order term to be small compared with the second-order one:

$$\left(\frac{\theta_{v.r.}}{\theta_c} + 1\right) \frac{R}{R_c} - \ln \left(\frac{16}{e^3} \ln \frac{e^{5/4} R}{2R_c}\right) \ll 1. \quad (\text{rainbow region}) \quad (84)$$

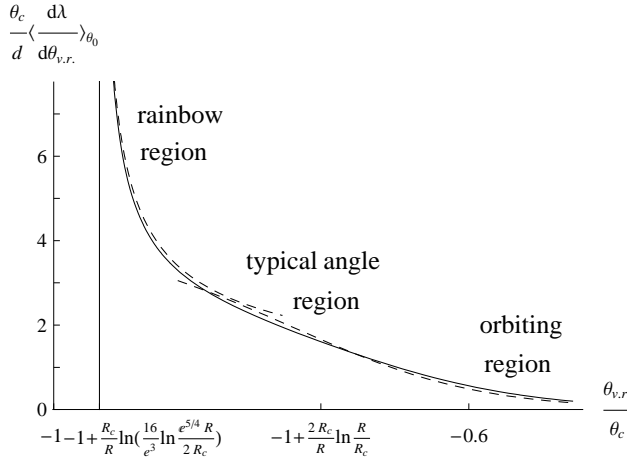


FIG. 9: The θ_0 -averaged differential cross-section of negatively charged particle scattering, at $R/R_c = 25$ (solid curve). The axes scales are chosen so that areas under the curve is unity, as the total probability. The left-hand dashed curve is evaluated by the approximate formula (83), the right-hand dashed curve – by the approximate formula (90). It is observed that those approximations in fact overlap.

Function (83) is shown by the left-hand dashed curve in Fig. 9.

b. Typical angle region. On the other hand, if $\nu^{(-)}$ is not too close to 1, i. e. under condition

$$\left(\frac{\theta_{v.r.}}{\theta_c} + 1\right) \frac{R}{R_c} - \ln\left(\frac{16}{e^3} \ln \frac{e^{5/4} R}{2R_c}\right) \gtrsim 1 \quad (\text{typical angles}) \quad (85)$$

opposite to (84), all the terms in (76) except the second logarithm (singular at $\nu^{(-)} \rightarrow 0$) may reasonably be approximated by their Taylor expansions up to linear terms – say, about the unit interval midpoint $\nu_{\text{mid}}^{(-)} = \frac{1}{2}$ [25]:

$$\theta_{v.r.} \approx -\theta_c \left[1 - \frac{2R_c}{R} \left(\ln \frac{\sqrt{3}R}{\nu^{(-)}R_c} - \frac{11}{6} - \nu^{(-)} \ln \frac{2R}{3e^{2/3}R_c} \right) \right]. \quad (86)$$

Then, for determination of the inverse function $\nu^{(-)}(\theta_{v.r.})$ one obtains the following simplified equation:

$$\left(\frac{\theta_{v.r.}}{\theta_c} + 1\right) \frac{R}{2R_c} + \frac{11}{6} \approx \ln \frac{\sqrt{3}R}{\nu^{(-)}R_c} - \nu^{(-)} \ln \frac{2R}{3e^{2/3}R_c}. \quad (87)$$

Here the r. h. s. is a monotonic function of $\nu^{(-)}$, so, in contrast to the exact equation (76), the simplified equation (87) has only one root (the second, lost root gives a small contribution to the differential cross-section). The solution to Eq. (87) expresses through the Lambert (product log) function $W(s)$ defined as a solution to equation $\ln s = \ln W + W$:

$$\nu^{(-)} \approx \frac{1}{\ln \frac{2R}{3e^{2/3}R_c}} W \left(\frac{\sqrt{3}R \ln \frac{2R}{3e^{2/3}R_c}}{R_c} e^{-\frac{11}{6} - \frac{R}{2R_c} \left(\frac{\theta_{v.r.}}{\theta_c} + 1\right)} \right) \quad (88)$$

(mind that $\theta_{v.r.}/\theta_c$ is negative and close to -1). From the definition of W , its asymptotic behavior in different regions derives as

$$W(s) = \begin{cases} s - \mathcal{O}(s^2) & s \ll 1 \\ \ln \frac{s}{\ln \frac{s}{\dots}} & s \gg 1 \end{cases} \quad (89)$$

and its derivative

$$W'(s) = \frac{1}{s(1 + 1/W(s))}.$$

Therefore, over the typical angle region the θ_0 -averaged differential cross-section is cast as

$$\frac{\theta_c}{d} \left\langle \frac{d\lambda}{d\theta_{v.r.}} \right\rangle_{\theta_0} = \theta_c \left| \frac{d\nu^{(-)}}{d\theta_{v.r.}} \right| \approx \frac{R}{2R_c \ln \frac{2R}{3e^{2/3}R_c}} \frac{1}{(1 + 1/W)}, \quad (90)$$

the argument of W being the same as in Eq. (88).

The full width of the differential cross-section as can be inferred from Eq. (90), and is obvious already from Eq. (76), amounts

$$\Delta\theta_{v.r.} \sim \theta_c \frac{2R_c}{R} \ln \frac{R}{R_c}, \quad (\text{neg. char. part.}) \quad (91)$$

which at $R/R_c > e^\pi \approx 23$ is larger than width (62) for positively charged particles.

The behavior of function (90) in region (85) is shown in Fig. 9 by the right-hand dashed curve. It describes the actual distribution quite accurately. In the orbiting region asymptotics, however, Eq. (90) errs by a factor of $e^{5/6}/\sqrt{3} \approx 1.3$ (see Eq. (93) below), so applicability of (90) is restricted by the bound

$$\frac{R}{2R_c} \left(\frac{\theta_{v.r.}}{\theta_c} + 1\right) \lesssim \ln \frac{R}{R_c} \quad (\text{typical angles})$$

in addition to (85).

One may anticipate formation of a shoulder in the distribution (90) at sufficiently large R/R_c , since then the argument of W can be large and $1 + 1/W \rightarrow 1$, making the differential cross-section $\theta_{v.r.}$ -independent. However, $W(s)$ reaches 5 ($\gg 1$) only at $s \sim 700$, so a shoulder in $\langle d\lambda/d\theta_{v.r.} \rangle_{\theta_0}$ may form up only at $R/R_c \gtrsim 100$.

c. Orbiting region. Finally, asymptotically large $\theta_{v.r.}$ are generated in the regions $\nu^{(-)} \rightarrow 0$ and $\nu^{(-)} \rightarrow 1$, where there are logarithmically rising terms in the relation (76). Examine first the region $\nu^{(-)} \rightarrow 0$. In this limit one may let $\nu^{(-)} = 0$ everywhere in (76) except in $\ln \frac{1}{\nu^{(-)}}$, and the reduced equation

$$\theta_{v.r.} \simeq -\theta_c \left(1 - \frac{2R_c}{R} \ln \frac{R}{eR_c \nu^{(-)}} \right)$$

is easily solved:

$$\nu^{(-)} \simeq \frac{R}{eR_c} e^{-\frac{R}{2R_c} \left(\frac{\theta_{v.r.}}{\theta_c} + 1\right)}. \quad (92)$$

Differentiating that expression by $\theta_{v,r}$, the differential cross-section asymptotics results as

$$\frac{\theta_c}{d} \left\langle \frac{d\lambda}{d\theta_{v,r}} \right\rangle_{\theta_0} \simeq \frac{R^2}{2eR_c^2} e^{-\frac{R}{2R_c}(\frac{\theta_{v,r}}{\theta_c} + 1)}, \quad (\text{orbiting region}) \quad (93)$$

provided

$$\frac{R}{2R_c} \left(\frac{\theta_{v,r}}{\theta_c} + 1 \right) \gg \ln \frac{R}{R_c}. \quad (\text{orbiting region})$$

As for the contribution from region $\nu^{(-)} \rightarrow 1$, which can be treated in a completely analogous manner, it equals

$$\frac{8R}{e^4 R_c} e^{-\frac{R}{R_c}(\frac{\theta_{v,r}}{\theta_c} + 1)},$$

and is definitely negligible compared to (93), so (93) is the complete asymptotic result.

V. HIGH-ENERGY LIMIT (PERTURBATIVE REGIME)

In conclusion, we will briefly comment on behavior of the function $\theta_{v,r}(b)$ in the opposite, high-energy limit,

$$\frac{d}{2\delta} = \frac{R}{R_c} \ll 1. \quad (94)$$

Thereunder, the deflection becomes perturbative (and better viewed in Cartesian coordinates, without the reference to a centrifugal force notion), and for positive and negative particles it must be equal in magnitude but opposite in sign. That is confirmed by Figs. 4 and Fig. 10.

The specific expression for the dependence $\theta_{v,r}(b)$ in this limit was obtained in [10] (Eqs. (18-19)), in the Cartesian coordinate framework:

$$\theta_{v,r}(\theta_0, b) \rightarrow \theta_{\text{Born}}(\theta_0, b) = \frac{1}{E} \int_{-\infty}^{\infty} dz F(b, z) \quad (95a)$$

$$= \pm 4 \frac{\sqrt{2Rd}}{R_c} \zeta \left(-\frac{1}{2}, \left\{ \frac{1}{2} + \frac{R}{2d} \theta_0^2 + \frac{b}{d} \right\}_f \right) \quad (95b)$$

(again, the braces indicate taking the fractional part). It involves the Hurwitz (generalized Riemann) zeta-function at a negative value of its first argument, which may be defined, e. g., as a contour integral [11]

$$\zeta(\alpha, v) = \frac{\Gamma(1-\alpha)}{2\pi i} \int_{-\infty}^{(0+)} \frac{s^{\alpha-1} e^{vs}}{1-e^s} ds \quad (96)$$

along a Hankel path [26]. Function (95b) is shown in Fig. 10 by dotted line. Note the identity $\zeta(-\frac{1}{2}, 0) = \zeta(-\frac{1}{2}, 1) (\equiv \zeta(-\frac{1}{2}))$, whereby function (95b) is everywhere continuous, with only a fracture point at $\frac{b}{d} = \frac{1}{2} - \left\{ \frac{R\theta_0^2}{2d} \right\}_f$.

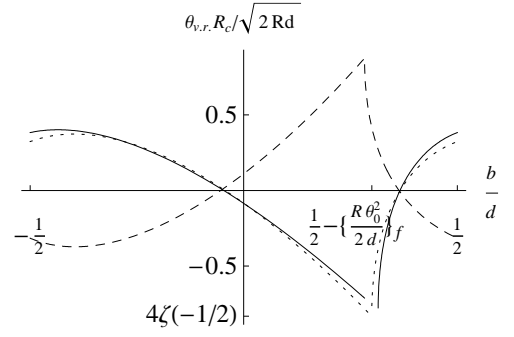


FIG. 10: Comparison of impact parameter dependences of the reflection angle for positive (solid curve) and negative (dashed curve) particles, at $R/R_c = 1/20$. Dotted curve – approximation (95b), for positively charged particles. The functions displayed may be continuously periodically extended beyond the interval $(-\frac{1}{2}, \frac{1}{2})$. The position of the fracture at $\frac{b}{d} = \frac{1}{2} - \left\{ \frac{R\theta_0^2}{2d} \right\}_f$ corresponds to tangency of the particle near-straight trajectory to one of the bent atomic planes.

The second argument of ζ -function in (95b) allows for a physical interpretation [10]:

$$b_{\text{ref}} = b + \frac{R}{2} \theta_0^2 \quad (97)$$

is the particle impact parameter at a depth where the particle straight trajectory becomes tangential to the bent atomic planes (actually, t_{ref}). Should one pass to b_{ref} instead of b , the dependence on θ_0 disappears completely:

$$\theta_{v,r}(\theta_0, b) = \theta_{v,r}(b_{\text{ref}}). \quad (98)$$

This contrasts with the case $R \gg R_c$ investigated in the previous section, where the θ_0 -dependence yet remained in a specific, casually located rainbow spike.

Here we will not contemplate demonstrating from expressions (36,50) that the limit of $\theta_{v,r}$ is indeed (95b). We only note that to this end one must implement significant cancellations between the pair of terms under the sum sign. One also notes that the second argument of ζ -function in (95b) is just the limit of $\nu^{(+)}$:

$$\lim_{\delta/d \rightarrow \infty} \nu^{(+)} = \left\{ \frac{1}{2} + \frac{R}{2d} \theta_0^2 + \frac{b}{d} \right\}_f. \quad (99)$$

For negative particles the route to (95b) is more intricate. In Fig. 10 we numerically compare approximation (95b) with the exact result – the agreement is quite convincing.

The comparison with the perturbative scattering pattern may also give an insight into the origin of the volume reflection phenomenon. The average of function (95) over the impact parameter b turns out to be strictly zero (see [10]) – hence, in the high-energy limit signatures of the volume reflection completely disappear. That owes to the fact that $\int_{-d/2}^{d/2} db F(b, z) \equiv 0$ at any given z (regardless of

the crystal bend). In contrast, at $R \gtrsim R_c$ the trajectory may *not* be viewed as merely straight [27], and the particle distribution is non-uniform over the crystal volume. In fact, “shadowed regions” not filled by the particles may appear at the inner side of bent potential ridges, in which the force acts in the positive direction. The deficit of a positively directed force on the beam then leads to the negative sign of the particle beam mean deflection angle.

VI. EXPERIMENTAL OBJECTIVES AND PARAMETER OPTIMIZATION

The alleged application of volume reflection is for high-energy particle beam extraction from accelerator beam-lines, when that is not manageable locally with laboratory magnets (intra-crystal forces are much stronger). Thereat, the beam parameters (energy and angular divergence) are given, while the crystal parameters have to be optimized in order to attain a suitable deflection quality.

The mean deflection angle

$$|\theta_{v.r.}| \sim \theta_c, \quad \theta_c = \sqrt{\frac{|F_{\max}|d}{2E}} \approx 0.25 \text{ mrad} \sqrt{\frac{\text{GeV}}{E}} \quad (100)$$

for a silicon crystal of orientation (110) depends only on the particle energy. The next parameter to care about is the angular spread acquired by the beam at the exit from the crystal. Neglecting the incoherent multiple scattering (to be estimated below), the spread $\Delta\theta_{v.r.}$, given by equations (62) and (91), for a given beam energy and crystal material depends only on the crystal bending radius. To set a criterion for beam solid deflection rather than spill, one may demand that the bulk of the dispersed beam (its both “edges”) be deflected to the same side. That implies:

$$R > 4R_c \quad (\text{for positively charged particles}) \quad (101)$$

and

$$R > 2R_c \ln \frac{R}{R_c}. \quad (\text{for negatively charged particles}) \quad (102)$$

Relation (101), for positive particles, was discovered previously by Maishev [5] based on numerical simulation studies. Our paper, thereby, offers a formal justification for that empirical relation, although within a framework of a simplified model. The emerging ratio

$$q = \frac{\max |\theta_{v.r.}|}{\Delta\theta_{v.r.}} = \begin{cases} \frac{R}{4R_c} & \text{for pos. charged particles} \\ \frac{R}{2R_c \ln \frac{R}{R_c}} & \text{for neg. charged particles} \end{cases} \quad (103)$$

quantifies the steering quality. But for the deflection to be significant practically, one moreover should have

$$q \gtrsim 3, \quad (\text{efficient deflection}) \quad (104)$$

entailing for the crystal curvature radius

$$R \gtrsim 10 \div 15R_c. \quad (105)$$

In demonstrational experiments [3] the latter requirement was marginally satisfied.

Next, concerning the crystal thickness (L), it is beneficial to make it low in order to minimize the multiple scattering. Evaluating the characteristic ratio [28]

$$\begin{aligned} \frac{\theta_x^{\text{mult}}}{\theta_c} &\approx \frac{13.6 \text{ MeV}}{\sqrt{2}E} \sqrt{\frac{2E}{|F_{\max}|d}} \sqrt{\frac{L}{93.6 \text{ mm}}} \\ &\approx 4 \sqrt{\frac{\text{GeV}}{E} \frac{L}{\text{mm}}}, \end{aligned} \quad (\text{Si (110)}) \quad (106)$$

we conclude that with $L \sim 1 \text{ mm}$ (as is typical for experiments been carried out [3]), and $E \gtrsim 100 \text{ GeV}$, the multiple scattering dispersion shall not spoil the deflection.

The lower bound for L results from the requirement that the volume reflection must have space to develop, whereby the crystal bending half-angle $\frac{L}{2R}$ needs be larger than the critical angle, so

$$L \gg 2R\theta_c = \frac{2R}{R_c} \sqrt{\frac{Ed}{2|F_{\max}|}} \approx \frac{R}{4R_c} 3.3 \mu\text{m} \sqrt{\frac{E}{\text{GeV}}}. \quad (107)$$

(volume reflection saturation)

Even at E as high as 1TeV the minimal thickness here amounts only $0.1 \text{ mm} \frac{R}{4R_c}$, so the optimal crystal thickness seems to be of the order of millimeter fractions. Such thin crystals have been prepared recently (as described in [12]).

Ultimately, it would be interesting to study the volume-reflected beam shape (evaluated in Sec. IV) under condition when it is not distorted by the multiple scattering, i. e. provided

$$\frac{\theta_x^{\text{mult}}}{\Delta\theta_{v.r.}} \sim q \frac{\theta_x^{\text{mult}}}{\theta_c} \ll 1. \quad (108)$$

If L is made $\sim 0.1 \text{ mm}$, and $E \sim 10^2 \div 10^3 \text{ GeV}$, that requirement is still achievable. However, besides the beam broadening in the target, the final beam spread can not be smaller than the initial width, $\Delta\theta_0$, determined by the beam focussing capabilities. Direct estimate of $\Delta\theta_{v.r.} \sim \theta_c/q$, with θ_c given by (100), and for $E \sim 100 \text{ GeV}$, $q \sim 3$ gives $\Delta\theta_{v.r.} \sim 10^{-5} \text{ rad}$. Hence, $\Delta\theta_0$ must be smaller than that degree. Actually, 10^{-5} rad are the lowest beam divergences practiced at modern accelerators, so significantly lowering them (even only along one direction, perpendicular to the active atomic planes) may be a challenging task. Vice versa, we may consider that as an extra motivation for the technology development.

VII. SUMMARY

In this paper, based on the model of a purely parabolic continuous potential in a bent crystal, an explicit ana-

lytic expression (26) for the trajectory of an over-barrier passing particle has been obtained, for cases of positive and negative particle charge. From the solution for the trajectory, the particle final deflection angle was derived as a function of the particle impact parameter and energy, in form of series (36, 50). Asymptotic behavior of those series at $R \gg R_c$ was explored, and asymptotic values for the volume reflection angle were found. They equal: $-\frac{\pi}{2}\theta_c$ for positive particles, and $-\theta_c$ for negative particles (in general accord with the existing results of numerical simulation with more realistic continuous potentials [2, 5, 6]).

For a more detailed description, the profile of the scattered beam has been evaluated in the simplifying limit $R \gg R_c$. In principle, the final beam profile may contain a visible admixture of boundary dependent effects (a θ_0 -dependent spike), which seemingly was not revealed by previous computer simulation studies. Fortunately, as we have shown, the boundary effects get completely erased in the differential cross-section averaged over a tiny interval of incident angles θ_0 (condition (67)), or, analogously, when subject to a small amount of multiple scattering. For positive particles, the θ_0 -averaged scattered beam has a table-shaped, flat distribution (Fig. 7) with the full width $\Delta\theta_{v.r.} = \frac{2\pi R_c}{R}\theta_c$. For negatively charged particles (Fig. 9) the angular distribution full width equals $\Delta\theta_{v.r.} \sim \theta_c \frac{2R_c}{R} \ln \frac{R}{R_c}$. The angular distribution in this case is asymmetric, exhibiting a spike on its edge, corresponding to the rainbow scattering, and an exponential tail on the opposite side, corresponding to orbiting. With the account of continuous potential smearing in vicinity of the atomic planes, we may expect that for positively charged particles there will appear features similar to those for volume-reflected negatively charged particles, only manifest much weaker.

As an instructive check, we also have verified (numerically) the correspondence of our generic calculation with the asymptotically high energy limit $R \ll R_c$ (Sec. V), where an analytic result was available. A rigorous proof of the correspondence is yet to be given. The straightness of the particle passage in this limit disallows any manifestation of the beam reflection as a whole, which should be borne in mind when interpreting the volume reflection phenomenon.

Finally, we made some numerical estimates (Sec. VI), which, we hope, may serve for planning further experiments in the field bent crystal-particle interaction. For the practical application of the beam volume reflection (including the multi-crystal setup) one has to work at increasing the parameter q given by Eq. (103). For fundamental investigation of the angular dispersion inherent to volume reflection dynamics one has to seek ways of diminishing the initial beam angular divergence $\Delta\theta_0$.

The derived representation for the particle trajectory may be used for description of various (weak) processes accompanying the particle passage – such as volume capture and electromagnetic radiation. The departures of the particle dynamics from the locally harmonic motion,

due to a more realistic form of the continuous potential, incoherent multiple scattering, etc., may, to some extent, also be studied on a perturbative basis. Yet, it would be useful to attain an analytic solution also for the case of (111) planar orientation, which involves alternating parabolic potential wells of different depth, compared to the presently considered (110) orientation when all the potential wells are identical.

Appendix A: Formal procedure of θ_0 -averaging

In Sec. IV A we had obtained, for positively charged particles, the scattering differential cross-section in form

$$\frac{d\lambda}{d\theta_{v.r.}} = \frac{R}{2\pi\theta_c R_c} \sum_m \frac{1}{|d\nu^{(+)} / db|_{b=b_m(\nu^{(+)}(\theta_{v.r.}), \theta_0)}}. \quad (A1)$$

Our objective now is to straightforwardly compute the sum involved hereat for the specific function $\nu^{(+)}(b, \theta_0)$ given by Eq. (35), first for an arbitrary θ_0 , and then average it over θ_0 , in order to justify our assertion that combined averaging over b and θ_0 (within tiny interval (67)) is equivalent to averaging over $\nu^{(+)}$.

To begin with, let us find the roots b_m explicitly. Eq. (35) is equivalent to

$$\frac{\tau^2\theta_0^2 + (b + \delta)^2 - \left(\frac{d}{2} - \delta\right)^2}{2\delta d} = \nu^{(+)} + m \quad (A2)$$

with m an integer, solution of which is straightforward:

$$b_m(\nu^{(+)}, \theta_0) = -\delta \pm \sqrt{2\delta d (\nu^{(+)} + m) + \left(\frac{d}{2} - \delta\right)^2 - \tau^2\theta_0^2}. \quad (A3)$$

Here the sequence of m begins with a smallest integer m_0 at which the radicand in (A3) is yet positive, viz.

$$m_0 = \left\lceil \frac{\tau^2\theta_0^2 - \left(\frac{d}{2} - \delta\right)^2}{2\delta d} - \nu^{(+)} \right\rceil + 1. \quad (A4)$$

The upper limit of m in Eq. (A3) equals to the largest integer at which yet $b < \frac{d}{2}$ (for a branch with the “+” sign in front of the root in Eq. (A3)), and $b > -\frac{d}{2}$ (for a branch with the “-” sign). That yields, correspondingly, values

$$m_{\max 1} = \left\lfloor \frac{\tau^2\theta_0^2}{2\delta d} - \nu^{(+)} \right\rfloor, \quad (A5)$$

$$m_{\max 2} = m_{\max 1} + 1. \quad (A6)$$

The number of terms in the sums from (A4) to (A5, A6) is large:

$$m_{\max 1,2} - m_0 = \frac{d}{8\delta} + \mathcal{O}(1) \equiv \frac{R}{4R_c} + \mathcal{O}(1) \gg 1.$$

Next, values of derivative $\frac{d\nu^{(+)}}{db}$ in points b_m are easily evaluated, noticing that the fractional part operator in

$\nu^{(+)}$ is inconsequential for derivatives [29]. Differentiating (A2) gives

$$\left. \frac{d\nu^{(+)}}{db} \right|_{b=b_m} = \frac{b_m + \delta}{\delta d}. \quad (\text{A7})$$

Identity

$$\frac{1}{\left| d\nu^{(+)}/db \right|_{b=b_m}} = \left| \frac{\partial b}{\partial m} \right| \quad (\text{A8})$$

suggests that upon substitution to (A1) one may expect

$$\begin{aligned} \left(\sum_{m=m_0}^{m_{\max 1}} + \sum_{m=m_0}^{m_{\max 2}} \right) \frac{1}{\left| d\nu^{(+)}/db \right|_{b=b_m}} &\approx 2 \sum_{m=m_0}^{m_{\max 1}} \frac{\partial b}{\partial m} \\ &\approx 2 \int_0^{d/2} db = d. \end{aligned} \quad (\text{A9})$$

as we anticipated in Sec. IV A, but to accommodate the dependence on θ_0 , we need to carry out the calculation more precisely.

Through (A3, A1), the differential cross-section assumes the form

$$\begin{aligned} \frac{d\lambda(\theta_{\text{v.r.}}, \theta_0)}{d\theta_{\text{v.r.}}} &= \frac{R}{2\pi\theta_c R_c} \\ &\cdot \left(\sum_{m=0}^{m_{\max 1}} + \sum_{m=0}^{m_{\max 2}} \right) \frac{\delta d}{\sqrt{2\delta d (\nu^{(+)} + m) + \left(\frac{d}{2} - \delta\right)^2 - \tau^2 \theta_0^2}} \\ &\approx \frac{d}{2\pi\theta_c} \sqrt{\frac{R}{R_c}} \sum_{m=0}^{R/4R_c} \frac{1}{\sqrt{m + \alpha (\nu^{(+)}(\theta_{\text{v.r.}}, \theta_0))}} \end{aligned} \quad (\text{A10})$$

with

$$\begin{aligned} \alpha(\nu^{(+)}(\theta_{\text{v.r.}}, \theta_0)) &= 1 - \left\{ \frac{\tau^2 \theta_0^2 - \left(\frac{d}{2} - \delta\right)^2}{2\delta d} - \nu^{(+)} \right\}_f \\ &\equiv \left\{ \frac{(b(\nu^{(+)}(\theta_{\text{v.r.}}, \theta_0) + \delta))^2}{2\delta d} \right\}_f. \end{aligned} \quad (\text{A11})$$

Outside the interval

$$-\frac{\pi}{2}\theta_c < \theta_{\text{v.r.}} < -\frac{\pi}{2}\theta_c \left(1 - \frac{4R_c}{R} \right), \quad (\text{A12})$$

there are no roots to equation $\nu^{(+)}(\theta_{\text{v.r.}})$, so the differential cross-section vanishes as an empty sum.

At a large upper limit the sum in (A10) grows as $\sqrt{R/R_c}$, whereas the difference

$$\sum_{m=0}^{R/4R_c} \frac{1}{\sqrt{m + \alpha}} - \sqrt{\frac{R}{R_c}} \xrightarrow{R/R_c \rightarrow \infty} \zeta\left(\frac{1}{2}, \alpha\right) \quad (\text{A13})$$

tends to a finite limit (it may be categorized as the Hurwitz, or generalized Riemann, zeta-function, see also definition (96)). Thereby, we may cast (A10) as

$$\frac{d\lambda(\theta_{\text{v.r.}}, \theta_0)}{d\theta_{\text{v.r.}}} \approx \frac{d}{2\pi\theta_c} \frac{R}{R_c} \left(1 + \sqrt{\frac{R_c}{R}} \zeta\left[\frac{1}{2}, \alpha(\theta_{\text{v.r.}}, \theta_0)\right] \right). \quad (\text{A14})$$

Here $\sqrt{R_c/R} \ll 1$, and the unity in parentheses (A14) corresponds to the result anticipated in (A9). But one should regard that at $\alpha \rightarrow 0$ function $\zeta\left(\frac{1}{2}, \alpha\right)$ blows up as $\frac{1}{\sqrt{\alpha}}$. So, the correction in the parentheses in (A14) can not be regarded as everywhere small.

Now, we turn to the issue that α is θ_0 -dependent. When θ_0 varies (at $\theta_{\text{v.r.}}$ fixed) even in a narrow interval (see (65)), α uniformly and repeatedly scans its definition interval from 0 to 1. Hence, the averaging over θ_0 is equivalent to the integration over α from 0 to 1. By virtue of the property

$$\int_0^1 d\alpha \zeta\left(\frac{1}{2}, \alpha\right) \equiv 0, \quad (\text{A15})$$

checkable from definition (A13), we have

$$\begin{aligned} \left\langle \frac{d\lambda}{d\theta_{\text{v.r.}}} \right\rangle_{\theta_0} &= \int_0^1 d\alpha \frac{d\lambda}{d\theta_{\text{v.r.}}} \\ &= \frac{Rd}{2\pi\theta_c R_c} \Theta\left(\theta_{\text{v.r.}} + \frac{\pi}{2}\theta_c\right) \Theta\left(-\theta_{\text{v.r.}} - \frac{\pi}{2}\theta_c\right) \left(1 - \frac{4R_c}{R}\right). \end{aligned}$$

Thereby, we arrive at equation (69), without any corrections $\sim \sqrt{R_c/R}$, q.e.d.

For negatively charged particles there arises a sum similar to that of (A1), though the dependence $\nu^{(-)}(b)$ differs a bit from $\nu^{(+)}(b)$. Nonetheless, the averaging procedure is completely analogous, the non-averaged differential cross-section equals (78) times the parentheses factor of (A14). Upon the θ_0 -averaging, through (A14) again, we arrive at Eq. (78).

[1] E. N. Tsyganov, Fermilab Report No. TM-682, 1976 (unpublished); Fermilab Report No. TM-684, 1976 (unpublished); V. M. Biryukov, Yu. A. Chesnokov, V. I. Kotov. Crystal Channeling and its Application at High-Energy Accelerators. Springer, Berlin, 1996.

[2] A. M. Taratin, S. A. Vorobiev. Nucl. Instrum. Methods B **26** (1987) 512-521; A. M. Taratin. Sov. J. Part. Nucl. **29** (1998) 437.

[3] Yu. M. Ivanov et al. Phys. Rev. Lett. **97** (2006) 144801; W. Scandale et al. Phys. Rev. Lett. **98** (2007) 154801.

- [4] W. Scandale et al. Phys. Rev. Lett. **102** (2009) 084801; W. Scandale and M. Prest, CERN Report No. CERN-SPSC-2008-014/SPSC-P-335, 2008.
- [5] V. A. Maishev. Phys. Rev. ST Accel. Beams **10** (2007) 084701.
- [6] W. Scandale et al. Phys. Rev. A **79** (2009) 012903.
- [7] J. Lindhard. Mat. fys. medd. Kgl. Danske vid. Selskab., **34** (1965) 14.
- [8] K. W. Ford, J. A. Wheeler. Ann. Phys. **7** (1959) 259; N. F. Mott, H. S. W. Massey. The theory of atomic collisions. Clarendon, Oxford, 1965; H. M. Nussenzveig. Diffraction effects in semi-classical scattering. Univ. Press, Cambridge, 1992.
- [9] G. V. Kovalev. JETP Letters **87** (2008) 87; arXiv:0712.0858.
- [10] M. V. Bondarenko, Phys. Rev. A **81** (2010) 052903.
- [11] F. W. J. Olver. Asymptotics and Special Functions. Academic Press, New York, 1974.
- [12] V. Guidi, A. Mazzolari, D. De Salvador, and A. Carnera, J. Phys. D **42** (2009) 182005.
- [13] C. Amsler *et al.* [Particle Data Group], Phys. Lett. B **667** (2008) 1.
- [14] Standardly [7], for a high-energy particle interacting with an oriented crystal, the particle wavelength shortness on the atomic scale makes the particle dynamics essentially classical, but yet non-perturbative, given the small angle of particle motion relative to a crystallographic direction and thus coherent action of atomic forces over long distances. Still, quantum effects may be viable in a special case when the particle transverse energy is very close to the height of an atomic potential barrier (the author is indebted to A.V. Shchagin for pointing this out in private conversation), but in any case, the classical calculation has to pave the way.
- [15] The crystal has to be thin in order to avoid the strong influence of multiple scattering, but still it may be thick enough for the volume reflection to occur within the crystal volume and be independent of the boundaries. We shall quantify this requirement later on.
- [16] The issue of the initial beam spread may be addressed after we derive the scattering differential cross-section.
- [17] At the very entrance to the crystal the force z -component may become comparable to x -component, in order to preserve the force nonvorticity but edge effects may certainly be neglected for a deeply penetrating particle.
- [18] The condition thereof is that the Thomas-Fermi radius of the material atom be commensurable with the interatomic distance half width. In silicon that is the case we have, but in crystals of heavier elements such as tungsten the atomic radius is appreciably smaller, and the parabolic approximation for the inter-planar continuous potential is poor.
- [19] Equation (1) in itself may apply to a non-ultra-relativistic motion, too, but physically, at lower energy there are larger effects of multiple scattering in the target, which we would like to neglect. So, we will actually imply the ultra-relativistic conditions in our paper.
- [20] Strictly speaking, the trajectory will not be exactly symmetric with respect to t_{reff} because the distances from t_{reff} to the crystal boundaries are in general different. However, contributions to θ_{reff} from crystal regions away from t_{reff} are supposed to decrease sufficiently rapidly, and one expects existence of a “thick crystal limit” of θ_{reff} , relevant in actual practice – see Sec. IV. In this paper, we content ourselves only to the “volume” contribution (33) to θ_{reff} and do not study any boundary effects. As we shall see later (Sec. IV and Appendix), however, the omission of boundary effects requires certain care.
- [21] Note that $\nu^{(+)}$ is a symmetric function of $b + \delta$ in the interval $-d/2 < b < d/2 - 2\delta$. That property in the following is transferred to the deflection angle as a function of the impact parameter.
- [22] $\nu^{(-)}$ is a symmetric function of $b - \delta$ in the interval $-d/2 + 2\delta < b < d/2$.
- [23] Equation (55a) agrees with our definition of the θ angle and differs in sign from the conventionally defined angle in a centrally-symmetric field.
- [24] In this subsection the sign alternative in $\frac{d}{2} \pm \delta$ corresponds to dealing with the first or with the second of the sums in (36b).
- [25] More elegant expressions, at the same time accommodating for a correct asymptotics in the orbiting region, result when the Taylor expansion is carried out about the point $\nu^{(-)} = 0$, but alas, that approximation would be definitely less accurate at typical $\theta_{\text{v.r.}}$.
- [26] Conventionally, the Hankel path is defined to begin in the complex s -plane at $-\infty$ ($\arg s = -\pi$), encircle the origin in the positive direction and return to $-\infty$ ($\arg s = +\pi$).
- [27] In the literature, sometimes one meets an interpretation of the volume reflection phenomenon exactly in terms of a straight trajectory tangential to the bent crystalline planes in some point. Such an interpretation, although satisfactory for a symmetric installation of crystals with a large bending angle ($\sim 2\theta_0 \gg \theta_c$), may be misleading for understanding of the underlying particle dynamics.
- [28] For the (rms, plane) multiple scattering angle upon the particle over-barrier passage we crudely apply a formula for the scattering angle in an *amorphous* target made of the same material (silicon): $\theta_x^{\text{mult}} = \frac{13.6 \text{ MeV}}{\sqrt{2}E} \sqrt{\frac{L}{93.6 \text{ mm}}}$ (as quoted in [13]).
- [29] Strictly speaking, differentiation of finite discontinuities will give δ -functional terms, but they will be imperceptible when inserted to the denominator of equation (63).